

Wireless Power Transfer System to charge an electric bike



Prepared by:
Xolisani Nkwentsha

Prepared for:
Professor M.A Khan
Department of Electrical Engineering
University of Cape Town

This report is submitted in fulfillment of the requirements of a
Bachelor of Science in Engineering in Mechatronics Engineering

22 October 2018

Declaration

We know that plagiarism is wrong. Plagiarism is to use another's work and pretend that it is one's own.

We have used the IEEE convention for citation and referencing. Each contribution to, and quotation in, this report/project from the work(s) of other people has been attributed, and has been cited and referenced.

This report/project is our own work.

We have not allowed, and will not allow, anyone to copy our work with the intention of passing it off as his or her own work.

Signature:

Xolisani Nkwentsha, NKWXOL003

22 October 2018

Terms of Reference

This project involves the design, simulation and implementation of a wireless power transfer system to charge a 12 V battery of an Electric bike.

DELIVERABLES:

1. Review of literature on state of the art wireless power transfer systems for electric bikes.
2. Conceptual design of WPT coils and power electronic system.
3. Experimental evaluation of the proposed system.

SKILLS/REQUIREMENTS: Interest in power electronics, Simulations in LT SPICE and ANSYS Maxwell.

AREA: Power electronics.

Acknowledgements

I would like to acknowledge Professor A. Khan, Sampath Jayalath, Edward, Maysam Soltanian, and the rest of the team in the Machines Lab and thank them for their support and guidance.

Abstract

Today, Wireless Power Transfer (WPT) is receiving an increasing amount of attention for providing wireless battery charge. With Potential to power devices that need a few Watts to devices that need kWatts. With applications in portable electronics, implanted medical devices, solar-powered satellites, unmanned aerial vehicles (UAVs), electric vehicle and many more. WPT is more convenient, less costly, and relieves the fear of running out of battery power.

This paper involves the design and implementation of a wireless power transfer system to charge a 12V battery for an electric bike. The design is split into electromagnetic and power electronic elements of wireless power transfer. The electromagnetic element involves the design of the transmitting and receiving coils for optimal power transfer. The power electronic element involves the design of circuitry necessary for wireless power transfer inverter such as an inverter, rectifier and voltage regulator.

The electromagnetic element is simulated in ANSYS Maxwell to design the transmitting and receiving coils, To obtain Inductance, Mutual inductance and Coupling coefficient between the coils. LT SPICE is used to simulate the power electronic elements and predict the transmission efficiency of the system from the designed coils.

The resulting efficiency of the system for a 10ohm load was 54% for a transmission distance of 50mm and 12% for a transmission distance of 100mm.

Contents

Declaration	i
Terms of Reference	ii
Acknowledgements	iii
Abstract	iv
Contents	v
List of Figures	vii
List of Tables	ix
1 Introduction	1
1.1 Background of the study	1
1.2 Objectives of the study	1
1.2.1 Problems to be investigated	1
1.2.2 Purpose of the study	2
1.3 Scope and Limitations	2
1.4 Plan of development	2
2 Literature Review	3
2.1 WPT Techniques	5
2.1.1 Inductive Coupling-based WPT	5
2.1.2 Magnetic Resonant Coupling-based WPT	5
2.2 Electromagnetics	7
2.2.1 Coil Shape	8
2.2.2 Coil and Core Material	9
2.2.3 Coil Alignment	10
2.2.4 Coil design	11

2.3	Power Electronics	12
2.3.1	Inverter Design	13
2.3.2	Compensation Network Design	16
2.3.3	Rectifier Design	17
2.3.4	Charging Method and Regulator Design	20
2.3.4.1	Charging Methods	20
2.3.4.2	Regulator Design	21
2.4	Applications: WPT	22
2.4.1	Electric Vehicles	22
2.4.2	Biomedical Implants	22
2.4.3	Portable Electronics	22
3	Methodology	23
3.1	Design	23
3.2	Theory Calculations	23
3.3	Simulations	24
3.4	Software	25
3.5	Experimentation	25
4	Design	26
4.1	System Overview	26
4.2	Electromagnetic Design	28
4.2.1	Coil Calculations	29
4.2.2	Inductance Calculations	30
4.2.3	AC resistance Calculations	30
4.2.4	Coil Implementation	31
4.3	Power Electronics Design	32
4.3.1	Inverter	32
4.3.2	Resonance	36
4.3.3	Rectifier	37
4.3.4	Regulator	39
5	Results	40
5.1	Simulations	40
5.1.1	ANSYS Maxwell	40
5.1.2	LT Spice	43
5.2	Practical Experimentation	48

5.2.1	Experiment 1: Transmission distance	49
5.2.2	Experiment 2: Switching Frequency	50
5.2.3	Experiment 3: Load	51
5.2.4	Experiment 4: Input Voltage	53
5.2.5	Mutual inductance calculations	54
5.2.6	Charging 12V Battery	55
6	Discussion	56
6.1	Self Inductance	56
6.2	Mutual Inductance	57
6.3	Transmission Distance	58
6.4	Switching Frequency	59
7	Conclusion	60
8	Recommendations	61
8.1	Resonance	61
8.2	Switching noise	61
8.3	Charging Method	61
8.4	Communication Protocol	61
8.5	Alignment	62
	Bibliography	63
A	Inverter Circuit	67
B	Gate Driver Circuit	68
C	STM32: PWM Code	69
D	12V Battery Datasheet	70

List of Figures

2.1	Overview of WPT techniques	3
2.2	Overview of a WPT System	4
2.3	Inductive Power Transfer generic circuit model	5
2.4	Magnetic Coupling Power Transfer generic circuit model	5
2.5	Basic illustration of wireless power transfer.	7
2.6	Common coil shapes for WPT	8
2.7	Angular misalignment and lateral misalignment between transmitter and receiver coils.	10
2.8	Power Electronics System: Inverter, Resonant Circuit, Rectifier and Voltage regulator.	12
2.9	Class E inverter.	13
2.10	bridge Class D inverters.	14
2.11	Class DE inverter.	15
2.12	Compensation networks: SS, SP, PP, PS.	16
2.13	Half wave rectification circuit	17
2.14	Full Bridge Rectifier circuit	18
2.15	Center tapped rectifier circuit.	18
2.16	Typical charging profile of a Lead-Acid battery.	20
4.1	Proposed wireless charging systems	26
4.2	Electric Bike in Machines Lab.	27
4.3	Circular coil configuration	28
4.4	Circular coil Implementation	31
4.5	Gate Drivers and Inverter Circuit	32
4.6	Inverter circuit diagram	33
4.7	Inverter Operation.	34
4.8	Flowchart for PWM code.	35
4.9	Series-Series Compensation topology.	36
4.10	Full Bridge Rectifier.	37

4.11	Full Bridge Rectifier in LT SPICE.	38
4.12	Full Bridge Rectifier Input and Output	38
4.13	Voltage Regulator Circuit.	39
5.1	Coils designed in ANSYS	40
5.2	Magnetic field around the coils: B Field	41
5.3	Mutual Inductance vs. Transmission Distance	42
5.4	Coupling Coefficient vs. Transmission Distance.	42
5.5	SS Compensated WPT system and it's equivalent T-Model.	43
5.6	Equivalent T-model for the Coils	43
5.7	Input (green) and Output (blue) Voltage for 50mm	44
5.8	Input (red) and Output (green) Current for 50mm	45
5.9	Input (blue) and Output (green) Voltage for 100mm	46
5.10	Input (red) and Output (green) Current for 100mm	46
5.11	Coils	48
5.12	Transmission Efficiency vs. Transmission Distance	49
5.13	Transmission Efficiency vs. Switching Frequency for 50mm	50
5.14	Transmission Efficiency vs. Switching Frequency for 100mm	51
5.15	Transmission Efficiency vs. Load Resistance for 50mm	52
5.16	Transmission Efficiency vs. Load Resistance for 100mm	52
5.17	Transmission Efficiency vs. Input Voltage, for 50mm	53
5.18	Transmission Efficiency vs. Input Voltage, for 100mm	54
5.19	Electric bike Battery	55
6.1	Ringing graph from inverter	58

List of Tables

2.1	Q-factors for different Topologies [1].	6
2.2	Inverter topologies.	15
2.3	Rectifier Types.	19
4.1	AWG Table	29
4.2	Calculated AC resistances at different frequencies.	31
4.3	Calculated capacitance for resonance.	37
5.1	Simulated Coil Parameters at 50mm transmission distance.	41
5.2	Parameter for LT Spice simulation for 50mm transmission distance.	44
5.3	Power transmission for 50mm	45
5.4	Power transmission for a 10 ohm load	47
5.5	Measured Coil Parameters	48
5.6	Input and Output for different transmission distances with 10V input voltage and 100kHz switching frequency.	49
5.7	Input and Output for different switching frequencies at 50mm.	50
5.8	Input and Output for different Load impedance for 50mm.	51
5.9	Input and Output for 50mm at 100kHz	53
5.10	Practical Mutual Inductance for different distances	54
6.1	Self Inductance from different methods.	56
6.2	Mutual Inductance from different methods.	57
6.3	Efficiency for different transmission distances with 10V input voltage and 100kHz switching frequency.	59
6.4	Efficiency for different switching frequencies	59

Chapter 1

Introduction

1.1 Background of the study

In the 19th century, Nikola Tesla invented the Tesla coil for a wireless power transfer system to provide wireless energy in the effort to create a “World Wireless System” to power the world, but was not able to make it fully functional due to financial problems. Wireless Power Transfer has been gaining a great deal of attention over the years [2]. The WPT technique has a wide variety of applications from charging cell phones to unmanned aerial vehicles, transferring power ranging from Watts to kilo-Watts.

Although conventional wire-based methods still offer more efficiency in the transfer of power. The WPT method is more convenient, less costly, and relieves the fear of running out of battery power. In the case of green and smart cities Electrical vehicle seem to be more modern and represent social progress, and WPT is the ideal solution for charging electrical vehicles. Electric-bikes are especially suitable due to the low amount of power stored in their batteries [3].

1.2 Objectives of the study

1.2.1 Problems to be investigated

The main objective of this study to implement a wireless power transfer system to charge a 12V battery for an electric bike. Steps that need to be taken to achieve the main objective are:

- Design and simulate the model of magnetic coils system using ANSYS Maxwell
- Design and simulate power electronic system in LT Spice
- Implementation and experimental evaluation of the proposed WPT system

1.2.2 Purpose of the study

Wireless Power Transfer has attracted large amount of interest due to its benefits and futuristic nature. The WPT technique has found applications in portable electronic devices, implanted medical devices, unmanned aerial vehicles, electric vehicles, etc. Large companies such as Apple and Sony are using WPT technologies in their products, such as Apple's iWatch with wireless charging [2]. WPT technology is exciting and can be used to attract learners to Electrical Engineering. The wireless power transfer system can be demoed during open day as one of the many exciting things Electrical engineering has to offer prospective students.

1.3 Scope and Limitations

Wireless power transfer can be implemented using multiple techniques, this report will be limited to inductive power transfer topologies. Due to time constraints the system is limited to 2 coil arrangement for wireless charging, other configurations will not be investigated. The main objective is to transfer power to charge the electric bike and not to necessarily optimise for large distance or high efficiency.

Wireless power transfer systems can provide low or high power with a wide range of applications. The scope of this report is limited to low powered wireless power transfer and the application is specifically the charging of a 12V battery for an electric bike and does not include other devices such as cell phones or batteries for electric cars even though WPT can be implemented for these devices. The project will not be designed for dynamic charging of electric bikes, which means that an electric bike cannot be charged in moving state.

1.4 Plan of development

The report begins with a survey of literature and theory development that is relevant to the design and implementation of a WPT system. This is followed by a methodology to summarize the design procedure. After this the system is designed through calculations and simulation. Then the system is implemented and experiments are performed to evaluate the performance of the WPT system. The results are then discussed and conclusions are made.

Chapter 2

Literature Review

Wireless Power Transfer(WPT) Technology has an ability of delivering power from a power supply to the load through air instead of wires. WPT commonly consists of the far-field and the near-field transmissions. The far-field WPT can be implemented by adopting the acoustic, the optical and the microwave as the energy carrier. The two most common near field techniques are inductive power transfer and magnetic Resonant Coupling [1]. Only near-field WPT techniques will be discussed in this paper. The highlighted parts in Figure 2.1 are for near field.

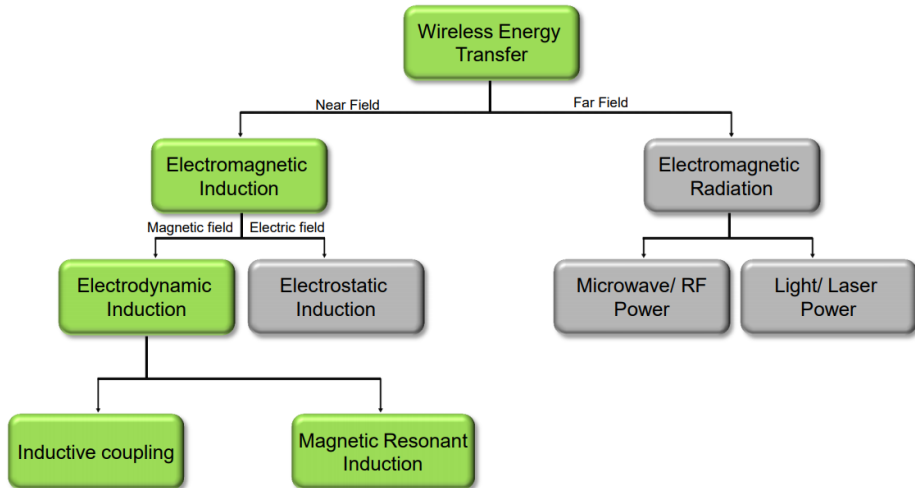


Figure 2.1: Overview of WPT techniques

The overall operation of a wireless power transfer system can be seen in figure 2.2. The system has two main parts: Power Transmitter and a Power Receiver. The power transmitter has a DC voltage supply, DC/AC Inverter and a transmitter coil. The power receiver has a AC/DC Rectifier, Regulator and load [4].

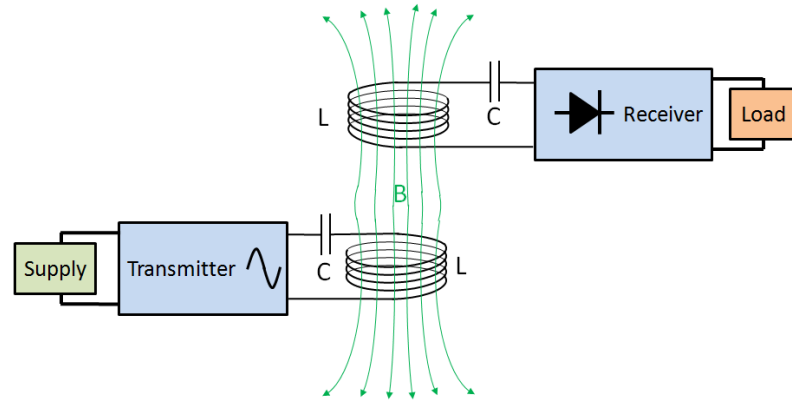


Figure 2.2: Overview of a WPT System

The operation of the WPT system follows the five following stages:

1. The Inverter converts the DC voltage from the DC supply to high frequency AC.
2. The alternating current goes to the transmitter coil.
3. The alternating current in the transmitter coil induces a magnetic field which extends to the receiver coil when its is close enough.
4. The magnetic field generates current in the receiver coil, which is converted to DC by the rectifier
5. the DC voltage supplies the load, hence power is transferred wirelessly

This Section provides a survey of literature on WPT techniques (i.e. Inductive Power Transfer and Magnetic Resonant Coupling), WPT power electronics (i.e. Inverter, Rectifier, Resonant and Regulator designs), WPT electromagnetics (i.e Coil Shape, material, size and alignment) and WPT application.

2.1 WPT Techniques

2.1.1 Inductive Coupling-based WPT

The Inductive coupling-based WPT uses magnetic induction to transfer power wirelessly. A common circuit configuration can be seen in Figure 2.3, where V_1 is the Supply voltage, R_1 and R_2 are the equivalent AC resistance of the coils, L_1 and L_2 are the inductances of the coils, Z_L is the load impedance, and M_{12} is the Mutual inductance between the transmitter and receiver coils [1].

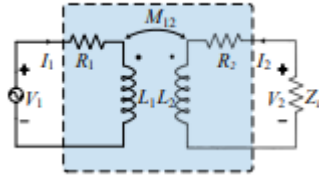


Figure 2.3: Inductive Power Transfer generic circuit model

This approach is very simple and offers high safety, and hence is widely used to charge mobile phones and laptops regardless of its short transmission distance (i.e. in centimeters range) and its low efficiency when the coils are not properly positioned [5].

2.1.2 Magnetic Resonant Coupling-based WPT

The Magnetic resonant coupling system is similar to the inductive system except the transmitter and receiver coils have to resonate at the same natural frequency. The natural resonant frequency enables the system to have a high efficiency [2]. Compared to the inductive approach, the magnetic approach's transmission distance is longer (i.e in meters range [5]) with higher efficiency.

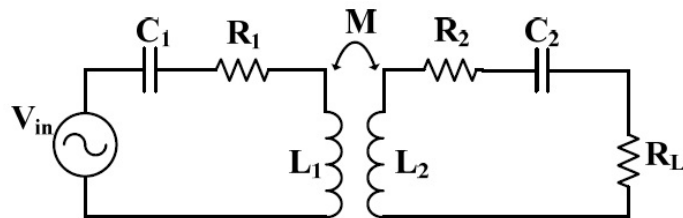


Figure 2.4: Magnetic Coupling Power Transfer generic circuit model

This approach usually has applications in Charging mobile devices, electric vehicles and implantable devices [5]. The most common circuit design for can be seen in Figure 2.4, where L_1 , L_2 , R_1 , R_2 , C_1 and C_2 are inductance of the coils, resistance of coil, and capacitance, R_L is the load and V_{in} is the supply voltage.

The efficiency for both systems depends on two key factors: The efficiency for both systems depends on two key factors: The efficiency for both systems depends on two key factors[1]:

1. The mutual inductance.
2. The Q-factors of the transmitting and receiving coils.

The mutual inductance can be given by:

$$M_{12} = k_{12} \sqrt{L_1 L_2} \quad (2.1)$$

Where k_{12} is the coupling coefficient between the transmitter and receiver coils. k_{12} changes as transmission distance changes [5].

There are four topologies that determine the Q-factor, namely series-series, series-parallel, parallel-parallel, parallel-series. Series-series is the topology shown in Figure 2.4. The Q-factor is indirectly proportional to efficiency and the Q-factor for this topology can be given by [6]:

$$Q = \frac{1}{R} \sqrt{\frac{L}{C}} = \frac{w_o L}{R} \quad (2.2)$$

Where w_o is the resonant frequency [2]. Q Factors for different topologies can be seen in Table 2.1.

Table 2.1: Q-factors for different Topologies [1].

Topology	Equations
SS	$\frac{w_o L}{R}$
SP	$\frac{R}{w_o L}$
PS	$\frac{w_o L}{R}$
PP	$\frac{R}{w_o L}$

2.2 Electromagnetics

When current flows through a conductor a magnetic field is produced. The relationship between the current and the field it induces can be obtained from Biot-Savart's law, which can be represented by Equation 2.3.

$$B(r) = \frac{u_0}{4\pi} \oint_C \frac{Idl \times r'}{|r'|^3} \quad (2.3)$$

where u_0 is the magnetic constant, I is the current in the conductor, and $r' = r - l$ is the full displacement vector.

When a conductor is placed in an moving magnetic field a current is induced and from Faraday's law which state: "a voltage is induced in a circuit whenever relative motion exists between a conductor and a magnetic field and that the magnitude of this voltage is proportional to the rate of change of the flux". Faraday-Lenz law can be represented by Equation 2.4.

$$\mathcal{E} = -N \frac{d\Phi}{dt} \quad (2.4)$$

Where \mathcal{E} is the induced voltage, N number of turns, and Φ is the flux. These are the two basic principles behind wireless power transfer. From Figure 2.5, coil 1 uses Boit-Savart's law to induce magnetic field, then coil 2 uses Faraday-Lenz law to induce power from the magnetic field.

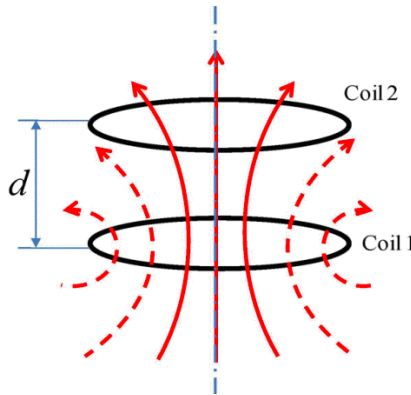


Figure 2.5: Basic illustration of wireless power transfer.

This section surveys the electromagnetic components involved in WPT to design and implement the WPT system to charge an electric bike. Several factors that affect the efficiency and transmission distance, these include Coil Shape, Material, Size and Alignment [2, 1].

2.2.1 Coil Shape

The coil shape is an important parameter that has an impact on efficiency and transmission distance. Different shapes are suitable for different applications. The most common coil shapes are planar and rectangular [7]. By turning the wire into a coil a concentrated magnetic field can be created. The coil can be circular, square, Hexagonal etc. and the configurations can be planar or Helix.

The Effects of coil shapes on efficiency, bandwidth and transfer distance for magnetic resonance coupling are studied in [8], where it was found that helix coils have the best performance while planar coils offer the worst performance.

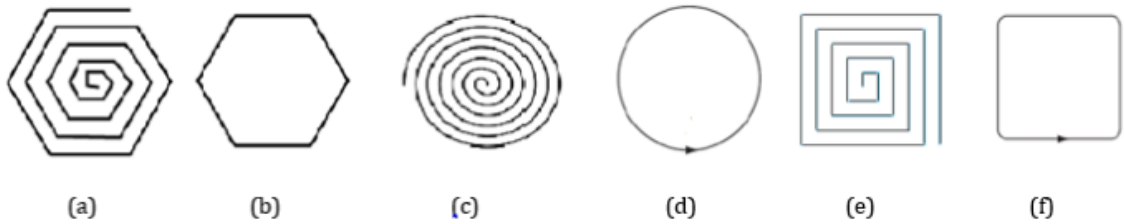


Figure 2.6: Common coil shapes for WPT

Common coils can be seen in Figure 2.6: planar Hexagon, helix hexagon, planar circle, helix circle, planar square and the helix square coil. The coupling coefficient k_{12} of the wireless power transfer system can be increased by using a spiral configuration, which in turn increases the mutual inductance and hence the transmission efficiency. The rectangular spiral coils are easy and simple to implement than the circular spiral coils [9].

In [10, 11], helix coils are used for wireless power transfer, while planar spiral coils are used for WPT in [12, 13, 14]. In [15, 16], square helix coils are used in the WPT.

2.2.2 Coil and Core Material

Wireless power transfer coils are linked by a core that acts as a path for the power to be transferred. The most popular cores are ferrite and air. In [17], a single-layer winding and receiver coil with cylindrical ferrite cores is used for wireless power transfer system. This system offers many advantages but has an extremely complex design.

Operating at High enough frequencies reduces the need for a magnetic core [18]. Switching frequencies in the hundreds of kilo-Hertz range eliminates the need for a magnetic core. The use of inductor coils with ferrite core is limited to low power applications, But inductor coils with air cores and laminated iron cores are applicable in medium to high power applications. The choice of the core material strongly affects the behavior of the inductor versus frequency [19].

Coil material has a significant impact of the transmission efficiency and distance. In [20], it was been shown that using a high Q planar-Litz coil can get almost 20% efficiency improvement. In [21], a magnetoplated wire (a copper wire that is plated with a magnetic thin film to improve transmission efficiency) has been used. In [22], multi-layer, multi-turn tubular coils have been adopted for improving the transmission efficiency, with a study of the skin-effect, and In [3] the material used is copper wire planar circular coils are used for an inductive power transfer system for 100W battery charging.

The ratio of transmitter diameter to transmitter distance can have a significant impact on the efficiency [2]. In [1], it is shown that if the twice the air gap is less than the coil diameter, the efficiency will be grater that 80%. The efficiency will decrease exponentially with an increase in transmission distance.

2.2.3 Coil Alignment

Wireless power transfer is based on the principle of electromagnetic induction, with the two main techniques - induction and resonance coupling. In both the receiver and transmitter coils need to be well aligned to achieve maximum efficiency.

Coil alignment has a great impact on transmission efficiency at a certain transmission distance. There are two types of misalignment between the transmission and receiver coil, namely angular and lateral in Figure 2.7. where angular misalignment is the transmitter and receiver coils are not parallel to each other, and lateral misalignment is when the centers of the coils are not aligned [2].

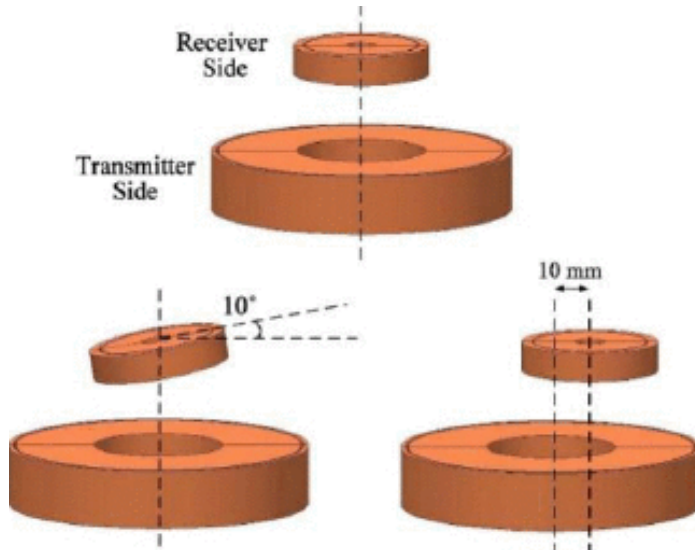


Figure 2.7: Angular misalignment and lateral misalignment between transmitter and receiver coils.

In [23], the effects of angular and lateral misalignment are studied and a four coil design is proposed to reduce the effects of misalignment. The four coil design was shown to be sufficiently robust for the considered application and operated within set limits for misalignment for a 1% tolerance in efficiency.

2.2.4 Coil design

The coil design is the most important component of a wireless power transfer system. The electromagnetic induction is heavily reliant on the coil configuration of the coil to achieve a high transmission efficiency. research is being done on coil configuration to improve efficiency.

In [24], an hollow planar spiral winding scheme was improved by using a non uniform track-width-ration with an increasing inner radius to improve the hollow planar and increase the q-factor, this method improved the efficiency by 20%.

In [25], an intermediate coil is used to boost the self inductance and magnetizing inductance of the transmitting coil at resonance frequency of the intermediate coil to compensate the coupling coefficient. The overall system in this paper has an efficiency of 95% for 200mm transmission distance.

[26] compares a two coil design to a U-coil design, and shows that the u-coil design is not only ten times more efficient than the two-coil system but it ensures the cleanliness of the space in the direction of the power transmission.

2.3 Power Electronics

The Power electronic systems needed for wireless power transfer are: inverter (DC to AC converter), resonant circuit, rectifier (AC to DC converter) and a voltage regulator as illustrated in Figure 2.8.

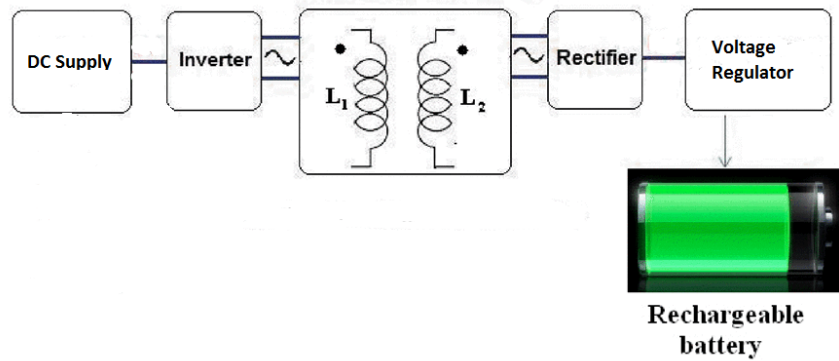


Figure 2.8: Power Electronics System: Inverter, Resonant Circuit, Rectifier and Voltage regulator.

The supply voltage of the system in Figure 2.8, the supply is DC source. For wireless power transfer to occur the current in the transmission coil needs to be AC to create a alternating magnetic field that will in turn induce an AC current in the receiver coil. At the terminals of the receiver coil an AC voltage will be induced, but charging (of mobile phones, laptop and EVs) requires a DC supply, which needs to be regulated.

The inverter converts the DC supply to high frequency AC for the transmission coil. The transmitter coil induces an alternating magnetic field for Boit-Savart's law. Then the receiver coil (when in the induced magnetic field) uses Faraday-Lenz law to induce AC Voltage at its terminals. The rectifier converts the high frequency AC from the receiver coil to DC for charging and the regulator ensure a constant supply from the wireless transfer system.

This section surveys the power electronic components involved in WPT to design and implement the WPT system to charge an electric bike.

2.3.1 Inverter Design

The Inverter converts DC from supply to high frequency AC for the transmitter coil. There are a number of topologies that can achieve this, most popular are Class E inverter, Class D half and full bridge inverter and Class DE inverter.

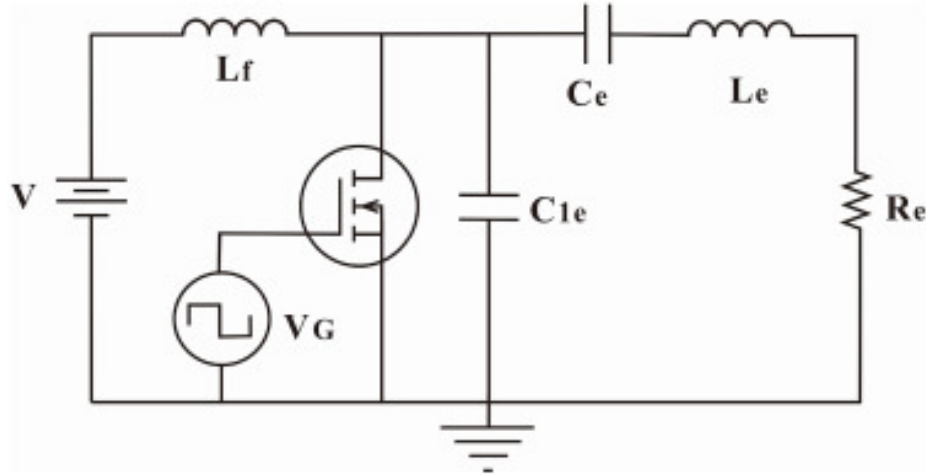


Figure 2.9: Class E inverter.

In Figure 2.9, A Class E inverter is shown. The Class E topology consists of two capacitors, two inductors, a switch, and the load.

The class E inverter is operated in switched mode - the transistor is driven to saturation to act as a switch that can either be on or off. The operation of the circuit is determined by the switch when it is on, and by the transient response of the impedance when the switch is off.

The simple single switch structure is popular for high power of several kilowatts and high efficiency at high operating frequency. For high power applications the class E can vary the output power using the duty cycle or switching frequency. The main disadvantage of this topology is the high voltage peak across the switch which means it will produce less power than other topologies for the same voltage and current. This high voltage peak may result in permanent damage [27].

Due to simple design, half and full bridge Class D inverters are the most popular in wireless power transfer applications [27], the half bridge Class D inverter is shown in Figure 2.10.

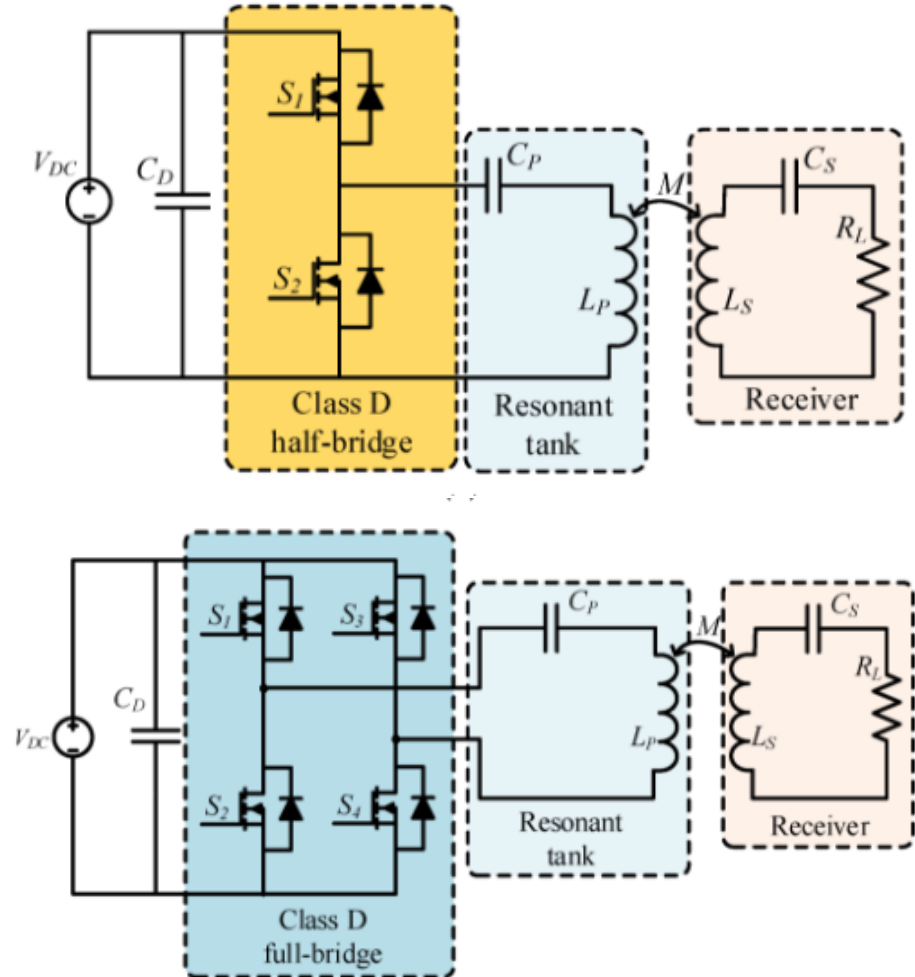


Figure 2.10: bridge Class D inverters.

The Class D inverter has two switches and an LC circuit configuration, and therefore has lower switching frequency than the Class E inverter. Due to the two switches this topology has less voltage stress across the switch than the Class E inverter. The peak voltage across the switch is twice that of the DC supply and hence it can output twice the voltage supplied to the LC circuit. This topology is suitable for low supply applications [27].

The class DE inverter topology in Figure 2.11. This topology combines the high efficiency of the class E inverter with the low switching stress of the Class D inverter. This topology is similar to the half bridge Class D inverter with the addition of capacitors in parallel with the switches as can be seen in Figure 2.11. This topology has a less switching losses, and enable high frequency operation with zero-voltage switching and zero-voltage derivative switching [27].

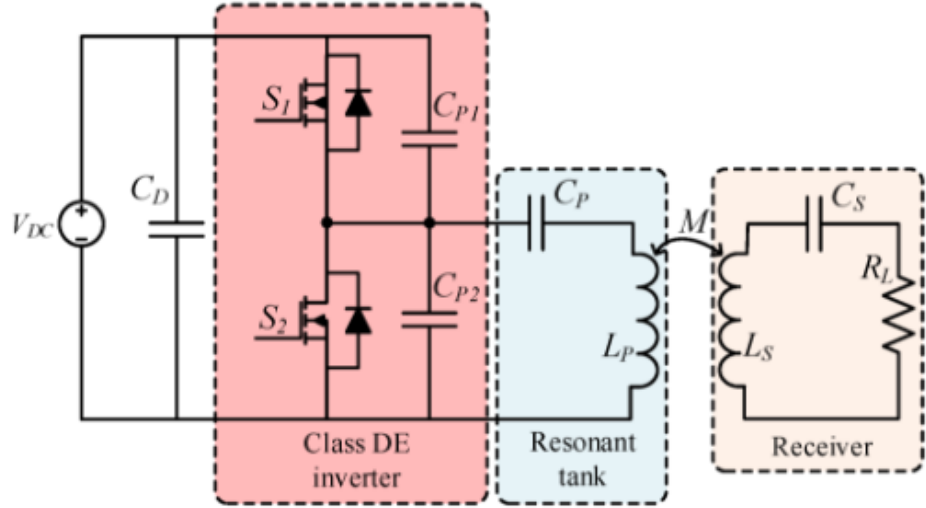


Figure 2.11: Class DE inverter.

In [3], the half bridge inverter is used implement a 100W battery charging system. In [28], the full bridge inverter is used to wirelessly charge electric bicycles. In [4], a full bridge inverter was used for a WPT system for electric vehicles. The characteristics of the inverter topologies discusses are summarised in Table 2.2.

Table 2.2: Inverter topologies.

Topology	Voltage Stress	Power Level	Frequency Operation	Switching Loss
Class E inverter	High	High	High	Low
Class D inverter	Medium	Medium	Medium	Low
Class D (full bridge) inverter	Medium	High	Medium	Low
Class DE inverter	Low	Medium	High	Low

2.3.2 Compensation Network Design

A compensation network is required to optimize the power factor of the wireless power transfer system [4]. The function of the compensation network is to illuminate the reactance in the system to ensure that all power is real. The compensation network has two capacitive elements to cancel out the inductive elements of the coils, with one connected to each coil. Based on the configuration of the capacitive element there are four topologies for compensation networks. The four topologies are shown in Figure 2.12, Series-Series (SS), Series-Parallel (SP), Parallel-Parallel (PP) and Parallel-Series (PS)

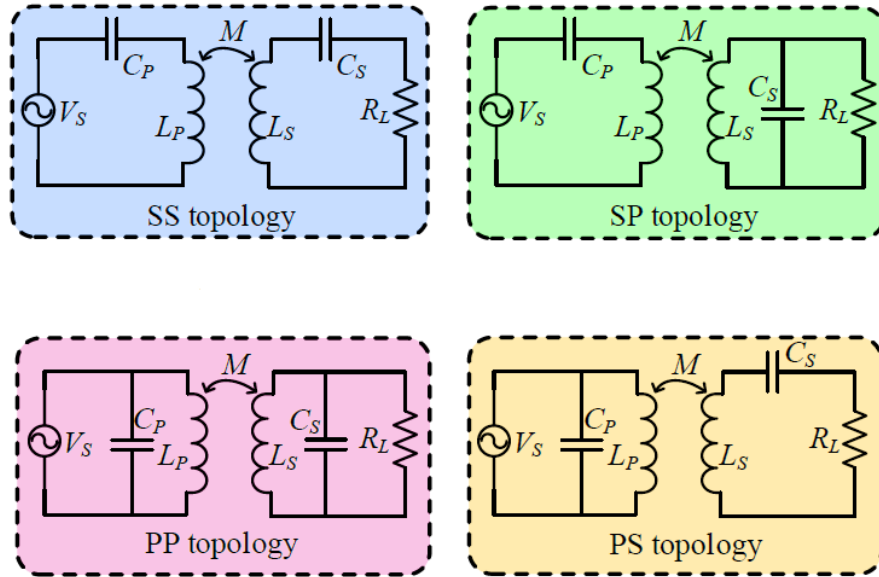


Figure 2.12: Compensation networks: SS, SP, PP, PS.

The Series-Series topology is most popular for practical application, it has a high tolerance of system parameters, and has no reflected reactance on the primary side [1]. The Series-Parallel topology is able to supply stable current. The Parallel-Series topology is able to supply a stable voltage [27].

The SS topology is more suitable for high frequency, low power and short distance applications. The SP topology is more suitable for low frequency, high power and long distance applications [29].

2.3.3 Rectifier Design

A rectifier converts AC to DC, the output can either be voltage or current with a pure DC or component of DC. Electric bike batteries need DC supply to charge, but the power produced by the secondary coil is AC. Therefore the system needs a rectifier to convert the AC from the coil to DC to charge the 12V battery. There are two types of Rectification: half cycle rectification and full cycle rectification.

Half cycle rectification has one circuit topology with a single diode to block the negative cycle, and therefore rectifying only the positive cycle. The circuit diagram for this topology is shown in Figure 2.13.

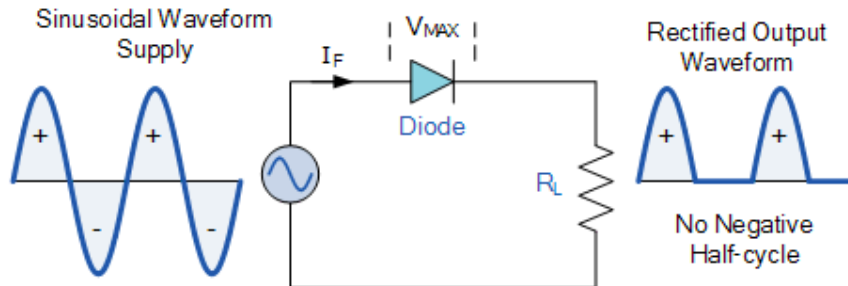


Figure 2.13: Half wave rectification circuit

Full cycle rectification has two topologies: full-Bridge and Center-tapped. half cycle rectification has a very low efficiency and a high ripple factor and is not common in wireless power transfer applications. full cycle rectification has a high efficiency and a low ripple factor and is most common in wireless power transfer applications.

The full bridge rectifier circuit can be seen in Figure 2.14. On the positive cycle of the supply diode D_1 and D_2 are operating and on the negative cycle diode D_3 and D_4 are operating. This effectively produces only positive values, as can be seen in Figure 2.14. The capacitor then filters the output waveform to a DC output with a ripple.

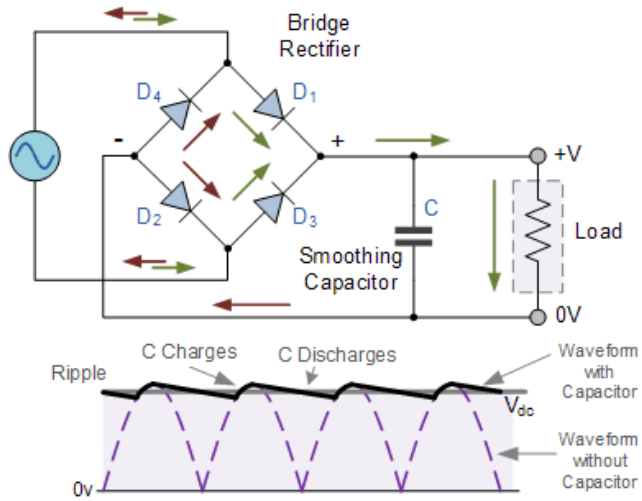


Figure 2.14: Full Bridge Rectifier circuit

The Center tapped rectifier circuit can be seen in Figure 2.15. On the positive cycle of the supply diode D_1 conducts and on the negative cycle diode D_3 conducts. This will produce the waveform shown in Figure 2.15.

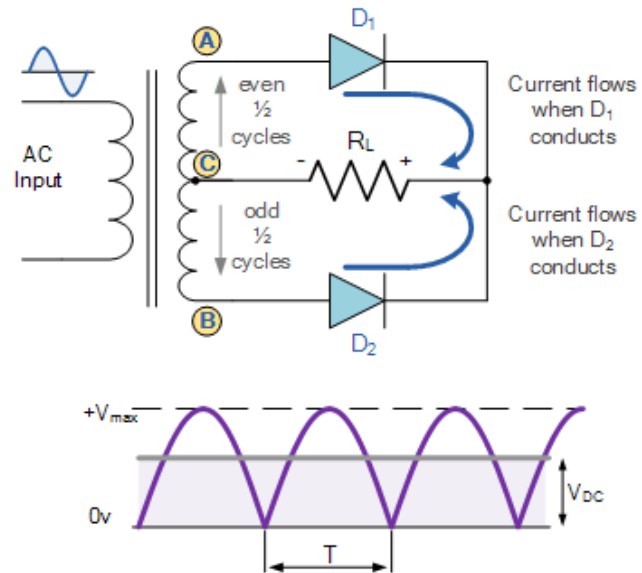


Figure 2.15: Center tapped rectifier circuit.

Center tapped uses two diode while full-bridge uses four, this means more voltage is lost over the four diodes of the full-bridge than the center tapped. Table 2.3, summarises that characteristics of the three rectification topologies discussed above

Table 2.3: Rectifier Types.

Parameter	Half-Wave	Center tapped	Bridge
No. of diodes	1	2	4
Max. efficiency (%)	40.6	81.2	81.2
Peak inverse voltage	V_{max}	$2V_{max}$	$2V_{max}$
Ripple factor	1.21	0.48	0.48
Output frequency	f	2f	2f
$V_{dc}(noload)$	$\frac{V_{max}}{\pi}$	$\frac{2V_{max}}{\pi}$	$\frac{2V_{max}}{\pi}$

[30], [31] and [28] use the full bridge rectifier to charge EVs. a circuit and overview of operation for a full bridge can be seen in figure 2.14 and the center tapped rectifier in figure 2.15.

All these topologies could have a diode or thyristor. there is no control signal required, and with a thyristor a control signal is required to allow forward current to flow.

2.3.4 Charging Method and Regulator Design

2.3.4.1 Charging Methods

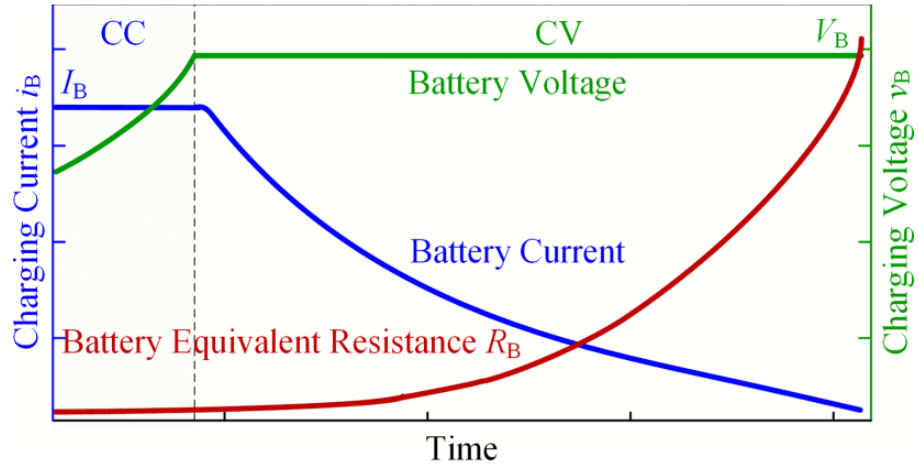


Figure 2.16: Typical charging profile of a Lead-Acid battery.

Rechargeable batteries are usually, the main power sources of electric bikes. The typical charging profile of a rechargeable battery is illustrated in Figure 2.16, where there are two different charging modes which include a constant current (CC) charging mode and a constant voltage (CV) charging mode. Initially, the battery is charged in constant current mode with the constant output current I_B , which is called charge current. While in CC mode, the battery voltage increase to the charge voltage V_B , and then the charging mode changes into constant voltage mode with the constant output voltage V_B . In CV mode, the charging current decreases exponentially until it reaches the end condition of charging, where the charging current is typically set as one-tenth of charge current. The battery load of wireless power transfer charging systems acts as an equivalent variable resistance R_B , which is the rate of charging voltage V_B over charging current I_B , as the red line shown in Figure 2.16. The aforementioned charging method is the CC/CV charging method, which is the most efficient and popular method for charging lead-acid batteries. [28]

Some battery charges use only one mode, meaning they are either operated in constant current mode or constant voltage mode [28].

CC/CV charging method is a conventional charging method which is used to charge lead-acid batteries. However, the lead-acid battery is being replaced by the lithium-ion battery in practice, because the lithium-ion battery has higher energy and power density.

Since the lithium-ion battery characteristics are clearly not the same as those of the lead-acid battery, the CC/CV strategy may be not the best charging method for the lithium-ion battery [32].

In [32], The three charging methods are compared. The criteria used to assess performance includes charging time, charging efficiency, and charging capacity. It was shown that CV charging has the highest charging time for less energy charging the battery. The charging capacities of the CV method and the CV/CC method are the same. The charging efficiency in the CC method is the highest for all these charging method.

2.3.4.2 Regulator Design

The level of voltage supplied to battery for charging is very important, if too much voltage is supplied then the battery will get damaged, and if the voltage supplied is too little the battery will not charge - in fact it could discharge. Current is also important as it determines the speed of charging, if the current supplied is too little then the battery might get damaged.

Basically, there are two types of Voltage regulators: Linear voltage regulator and Switching voltage regulator. A linear voltage regulator acts like a voltage divider with a resistance that varies with load to produce a constant output voltage. A switching regulator switches on and off rapidly the switching frequency determines the output voltage.

A linear regulator has a low output ripple voltage and a fast response time to load changes, but has a very low efficiency and required heat sinks since it heats up. A Switching regulator is more efficient and is capable of handling higher power, but it has a higher ripple voltage and slower recovery time. A Linear regulator although inefficient it has a much simpler design and is inexpensive.

2.4 Applications: WPT

Wireless power transfer has applications in a wide variety of fields ranging from medical to the automotive industry. wireless power transfer is currently being used for charging electric vehicles (cars, bikes etc.), household appliances etc.[33]

Major application of wireless power transfer is in portable electronics such as laptops, tablets and cellphones. The major application of WPT is in solar power satellites. wireless power transfer is also used in aircrafts, robots and rockets [33].

It is projected to have a wireless power transfer market will be worth \$17.04 Billion by the year 2020.

2.4.1 Electric Vehicles

For electric vehicle there is static charging and dynamic charging[1]. static charging for when the vehicle is stationary. currently alignment is a problem - therefore the device needs to be parked in a specific position for optimal charging. For dynamic charging, vehicles constantly get charged while on the road.

2.4.2 Biomedical Implants

Implantable medical devices have been growing as a way to assist people with dysfunctional organs. Wireless power transfer offers the most effective and convenient way to power these devices. Already a large amount of research has gone into applications of wireless power transfer in bio-medical implants [1].

2.4.3 Portable Electronics

Due to the disadvantage of tangled and inconvenient charger wires, the wireless power transfer has a promising future in portable electronics. Major companies like Apple and Sony have already produced wireless charged for their devices[1].

Chapter 3

Methodology

This section summarises the methods used in the implementation of the WPT system.

3.1 Design

To define design requirements, the system objectives are used. Certain factors such as time constraints, component availability and cost had to be considered to ensure that the design requirements are realistic and achievable. The practical application of the system was the main driver for design requirements.

To Design the system, a large amount of literature had to be reviewed to assist in making accurate design choices where time and availability were not constraints. The design was split into two parts which are power electronics and electromagnetics. The power electronics part involves the design of an Inverter, Rectifier, Regulator and compensation network. The electromagnetic part is the coil design to determine parameters such as coil shape, coil material etc.

3.2 Theory Calculations

From the theory surveyed, certain calculation were made to assist in the design. In the Electromagnetic design the American Wire Gauge was used to calculate the number of strands needed for the litz configuration to handle a certain amount of current.

Theory offered multiple formulae to calculate self inductance of the transmitter and receiver coils. The expression based on Current sheet approximation was used to calculate the inductance. Certain parameters were needed to determine the inductance of a coil such as wire material, wire diameter, coil shape, number of turns etc.

For Resonance, capacitor values required was calculated for a specific frequency. This method needs the inductance to have been computed and switching frequency to have been selected.

3.3 Simulations

Simulations were used to aid in designing and modelling the wireless power transfer system. The software packages used to simulate the system are ANSYS Maxwell and LT SPICE.

ANSYS Maxwell was used to simulate the electromagnetic performance of the system. This means that the software assisted in designing a 3D model of the coils and predict relevant parameters of the coils such as self inductance, mutual inductance and coupling coefficient. These parameters as mention in the literature review all affect the transmission efficiency of a wireless power transfer system. ANSYS Maxwell is a commercial software that is available in the computers in the engineering labs, therefore simulations were run in the labs.

Simulations on the ANSYS Maxwell Software were ran in the Green Lab, the PC specification for the Green lab computers are:

- Processor - Core i7 4790 @3.60GHz
- Memory - 16GB,DDR3 1600MHz
- Operating System - Windows 10 Enterprise, x64

LT SPICE was used to simulate the electronics involved in the wireless power transfer system. The software assisted in determining parameters such as input voltage, input current, output voltage, output current, power and efficiency. This software was also used to predict efficiency and output power for the designed system. LT SPICE is a free software, therefore it was possible to download the software and simulate from any computer.

Simulations on LT SPICE were ran on a computer with the following specifications:

- Processor - Core i5 4590 CPU @3.30GHz
- Memory - 16GB, DDR3 1600MHz
- Operating System - Windows 10 Home, x64

3.4 Software

The inverter requires two PWMs. To produce these signals the STM32FO micro controller was used. The programming language used was C. Atollic True Studio software was used to program the microcontroller to produce the desired PWM signals.

3.5 Experimentation

Experimentation was performed to evaluate the system the was implemented. Four experiments were performed to evaluate the effect of certain parameters to the system's transmission efficiency. The parameters were transmission distance, switching frequency, load resistance and input voltage.

The instruments used to measure the systems performance and supply power are listed below:

- Measured inductance and internal resistance using ISO-TECH, Model LCR-821 Meter 99999F, 99999 k, 99999h Bench Type.
- Measured current using an ISO-TECH ICM2000 Clamp Meter, Max Current 2.5kA ac, 2.5kA dc.
- Measured DC voltage using Gossen Metrawatt M249A Metra Hit Energy Single-Phase Power Quality Logger Multimeter.
- Measured AC voltage waveforms using Agilent 54621A Oscilloscope
- Supplied 12V to mosfet drives using a Escort Triple output dc supply
- Supplied input voltage for power transfer using AIM-TTI INSTRUMENTS QPX1200SP 1200W 60V 50A Single Output PowerFlex DC Bench Power Supply

Chapter 4

Design

This section will provide the design method, topology selection, and system calculations to design a wireless power transfer system to charge an electric bike. The system overview will firstly be discussed to clarify the scope and purpose of the design.

4.1 System Overview

In a future of environmentally friendly innovations, electric vehicles represent the way to go with respect to social progress and sustainability. For an easy and effective charging method of electric vehicles, wireless power transfer is the ideal solution.

The objective of this paper is to design charging station for electric bikes. An illustration of the system can be seen in Figure 4.1. The system has a charging pad that can charge the electric bike while it is parked. The transmitting coils would be on a pad on the ground, the magnetic field created by the transmitter coil will induce a current in receiver coil attached to the bottom of the electric bike. The receiver coils connected to a rectifier to provide a DC power for charging a battery.

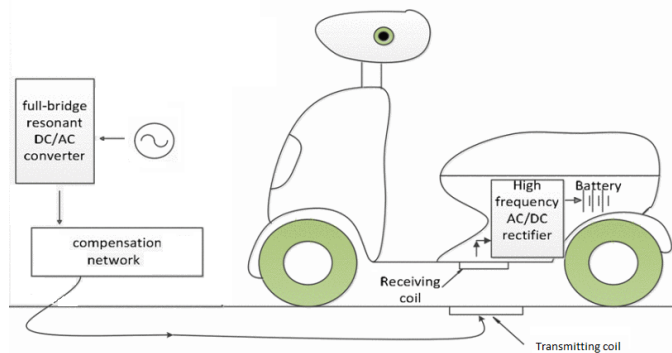


Figure 4.1: Proposed wireless charging systems

The transmission distance required for this system will be in the range 50mm - 120mm, this is the typical distance from the ground to the bottom of the electric bike. The typical batteries in electric bikes have a capacity of 12V.

The bike in the Machines lab, in Figure 4.2 will be used for designing the wireless charging system. This electric bike has two 12V 38AH/20HR lead-acid batteries, and will require the transmission distance to be 100mm. The system is designed for charging while at home or work for an average amount of 12 hours for a full charge cycle. From the 12V 38AH/20HR lead-acid batteries datasheet the system will require about 14.4V to 15V to achieve the desired charge cycle. The coil will have a 200mm diameter, Due to the dimensions of the electric bike in the Machines Lab.



Figure 4.2: Electric Bike in Machines Lab.

The Design requirement for the wireless system to charge a 12V battery for an electric bike can be summarised as follows

- Output Voltage in the range 14V-15V
- Transmission distance between 50mm and 120mm
- The coil dimensions must be 200mm x 200mm

4.2 Electromagnetic Design

The system will use a magnetic resonant coupling-based wireless charging, which requires the transmitter and receiver coil to resonate at the same frequency. Resonance eliminated the reactance by introducing capacitive elements to cancel the effect of inductive elements in the circuit to optimise the power factor of the system. This technique is the most suitable because it offers higher efficiency and longer transmission distance.

Although circular planar coils do not offer the best performance in efficiency and transmission distance, they will be selected for the system because they are simple for simulation, design, implementation. Copper wires in a Litz configuration will be used, due to its availability in the Machines Lab. From the reviewed literature, the selected switching frequency range will be 90kHz - 100kHz to eliminate the need for a magnetic core.

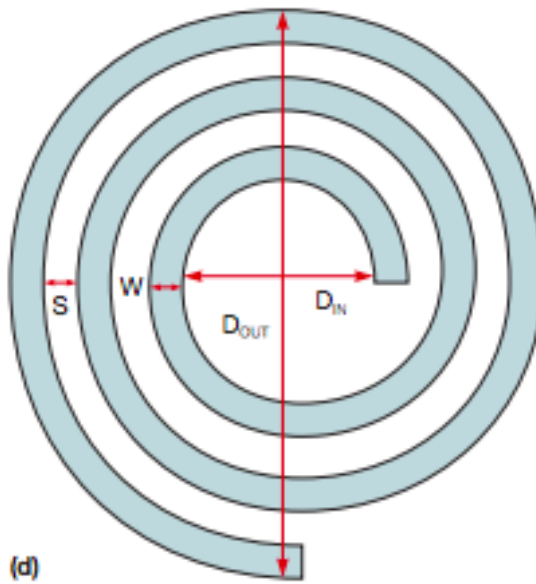


Figure 4.3: Circular coil configuration

4.2.1 Coil Calculations

The litz wire configuration for the coil has to be designed to handle 4A. The frequency for 100% skin depth will also be considered. Wires available in the Machines lab have a diameter of 0.5mm. The American Wire Gauge (a standardized system for defining the diameter of conductive wires) is used to determine characteristics of the wire from it's diameter.

Table 4.1: AWG Table

AWG Gauge	Diameter [mm]	Maximum amps for power transmission	Maximum frequency for 100% skin depth for solid conductor copper
0000	11.684	302A	125 kHz
...
24	0.51054	0.577A	68 kHz
25	0.45466	0.457A	85 kHz
...
40	0.07874	0.0137A	2900 kHz

The AWG table offers a wide range of wire diameters. Wire diameter 0.5mm is between AWG gauge 24 and 25, as can be seen in Table 4.1. The exact parameters for a 0.5mm diameter wire will be obtained with linear interpolation. From linear interpolation the maximum current and frequency was calculated to be 0.554A and 71kHz respectively.

For 4A, 7 strands in a litz configuration are required. To be safe 8 strands will be used. With All 8 strand together the new wire diameter was calculated to be 1.414mm and with 8 strands the coil can handle a maximum current of 4.4A.

4.2.2 Inductance Calculations

The multiple ways to calculate the inductance for a planar coil. The most popular method due to its simplicity and accuracy is the expression based on Current sheet approximation. The expression can be seen below,

$$L = \frac{u_0 n^2 d_{avg} c_1 p}{2} (\ln(c_2/p)/p + c_3 + c_4 p) \quad (4.1)$$

Where d_{avg} is the average between d_{in} and d_{out} in Figure 4.3, u_0 is the permeability of free space which is equal to 4×10^{-7} , n is the number of turns of the coil and the c_i are coefficients that are layout dependent. For a circular configuration $c_1 - c_4$ are 1, 2.29, 0 and 0.2 respectively. p is the fill ratio that can be expressed as:

$$p = \frac{d_{out} - d_{in}}{d_{out} + d_{in}} \quad (4.2)$$

Initially both coils were going to have 20 turns with an inductance of $26.14\mu H$, but due to availability in the machines lab, both coils will have 10 turns. The self inductance was calculated to be $19.01\mu H$.

4.2.3 AC resistance Calculations

The AC resistance for a coil can be calculated using the conductor's resistivity, the length of the conductor and the effective cross sectional area used by the skin effect using the equation below.

$$p = \frac{pl}{A_{eff}} \quad (4.3)$$

Where p is the resistivity of copper, l is the length of the wire, and A_{eff} is the effective cross sectional area. The effective cross sectional area used due to skin effect can be calculated by several methods with varying degrees of accuracy. The simplest method has the following expression.

$$A_{eff} = d \times \pi \times \text{diameter} \quad (4.4)$$

Where d is nominal depth of penetration for the wire, which can be expressed as.

$$d = \sqrt{\frac{p}{\pi \times f \times u}} \quad (4.5)$$

where f is the switching frequency, p is the resistivity and u is the absolute permeability. The AC resistance was calculated for three frequencies in the range 90kHz - 100kHz.

Table 4.2: Calculated AC resistances at different frequencies.

Frequency	AC Resistance
90kHz	0.0662
95kHz	0.0678
100kHz	0.0693

4.2.4 Coil Implementation



Figure 4.4: Circular coil Implementation

To implement the coil, two A4 perspex sheets were cut into 200mm x 270mm rectangles. 3mm diameter holes were made 10mm from the corners - to be used for building a structure for the wireless power system. Double sided tape was used to attach the coil to the perspex. The final coil can be seen in Figure 4.4

4.3 Power Electronics Design

The Machines Lab has a full bridge inverter available, due to time constraints it will be used to convert the DC input to high frequency AC signal for wireless power transfer. Series-Series topology will be used for the compensation network because it is the most suitable topology for high frequency, low power and short distance application [29]. As discussed in the section 2.3.2

The full bridge rectifier has a higher efficiency than the half bridge and is easier to implement than the center tapped rectifier. The full-bridge topology will be used for the rectification of the high frequency AC signal from the receiver coil to produce a DC signal for charging. Linear Voltage regulator will be used due to its availability in the Machines lab.

4.3.1 Inverter

The full bridge inverter in the Machines Lab uses the IRFP260N mosfet. This mosfet is rated 200V, 50A. These mosfets require 15V to power them, therefore mosfet gate drivers will be required. The mosfet gate drivers take in 12V and produce 15V. The mosfet drivers are provided by the Machines Lab. The circuit diagram for the inverter and gate drivers can be seen in appendix A and B respectively.

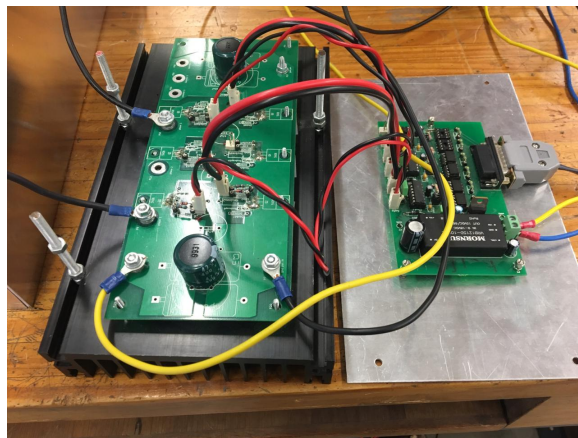


Figure 4.5: Gate Drivers and Inverter Circuit

The full bridge inverter has four mosfets that act as switches to produce an AC signal. The basic operation of this inverter is that only two diagonally opposite mosfets are ON at a time.

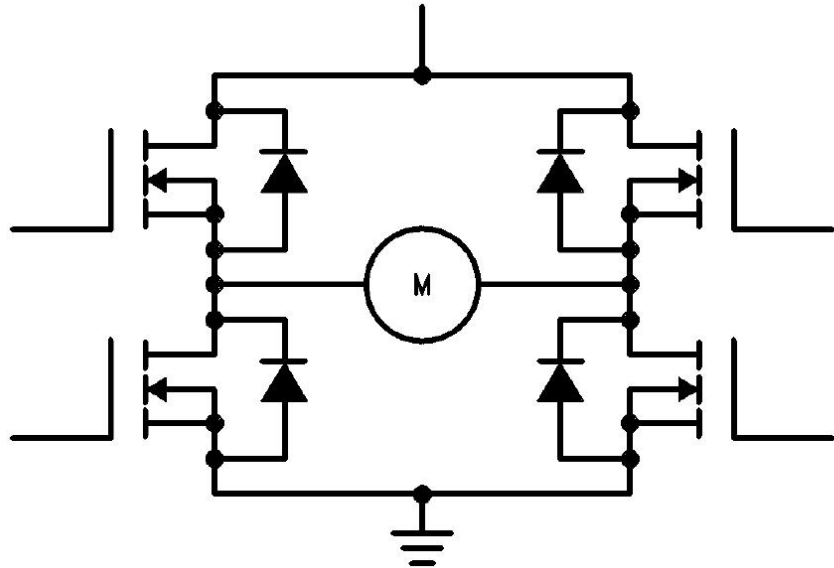


Figure 4.6: Inverter circuit diagram

The inverter will require two gate drivers, for each mosfet leg. where mosfet 1 and 2 are the left leg and while mosfet 3 and 4 is the right leg, as can be seen in figure 4.6. The gate driver produces two signals - one low, and one high. such that each leg has one mosfet on at a time. To prevent shorting and possible damage to the mosfets.

When the left leg driver sends a high to mosfet 1 and a low to mosfet 2, the right leg driver will send a high to mosfet 4 and a low to mosfet 3. The current will flow through the load from left to right as can be seen in Figure 4.7 with mosfet 1 and mosfet 4 conducting. When the gate driver switch, signals are inverted and the current will flow through the load from right to left and mosfet 2 and 3 will conduct. With fast switching an AC signal is generated at the output.

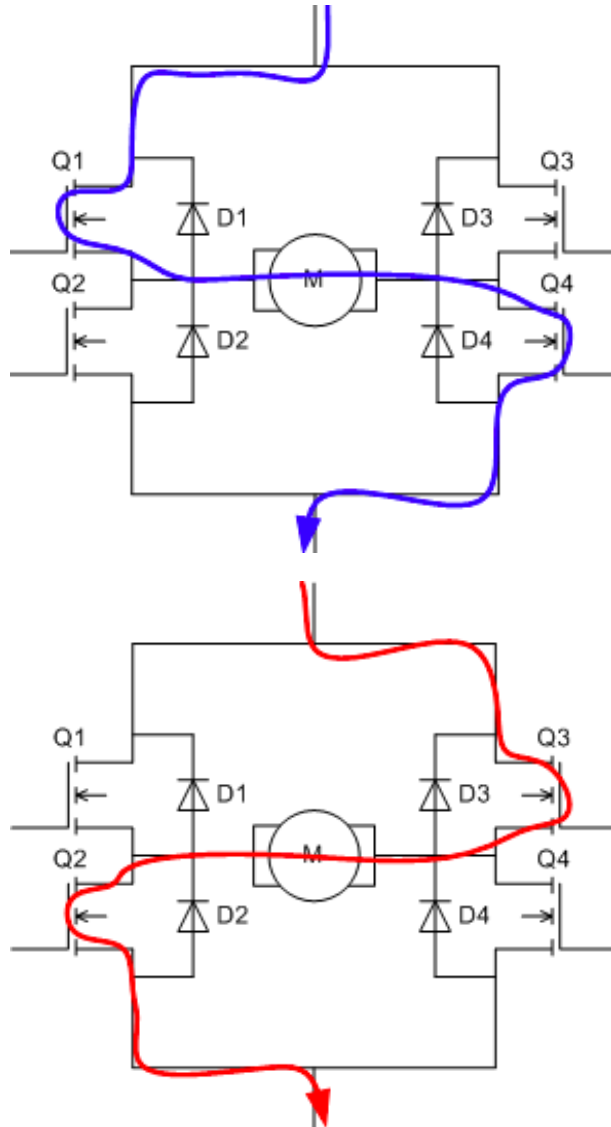


Figure 4.7: Inverter Operation.

For fast switching a pulse width modulated (PWM) signal is supplied to each gate driver. The PWM signals for the gates need to opposite for the inverter to operate. The full bridge inverter requires that there is dead-time between the switching of the signals to ensure that mosfets on the same leg are not on at the same time. To produce these PWMs the STM32F051C6 micro-controller is used. Atollic True Studio was used a software to code and interface with the STM micro-controller to produce the PWM signals with the required dead-time of about 200ns. Appendix C has a link to the github repository with the PWM code used.

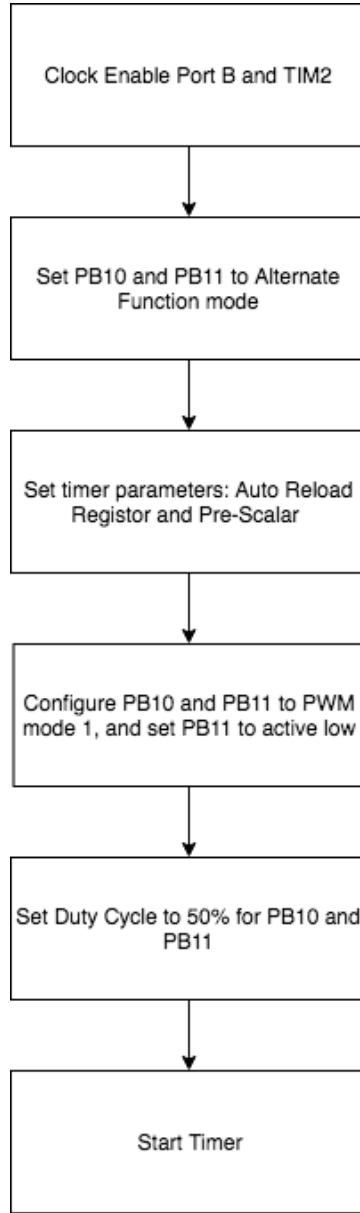


Figure 4.8: Flowchart for PWM code.

The code setup required the initialisation of Timer 2 to produce the PWM signals and port B for the output pins. Port B and timer 2 are clock enabled. Then the pins on port B (PB10 and PB11) are configured to alternate function mode to map them to the PWM channels (channel 3 and channel 4). The PWM parameter are configured to set the PWM frequency, resolution and state. These PWM parameters are the Auto Reload Register and Prescalar. The Prescalar attenuates the internal clock frequency, and the Auto reload register determined the number at which the system counter will reset. These two parameters determine the output frequency.

4.3.2 Resonance

The Series-Series topology has been chosen to increase efficiency. The purpose of the resonant circuit is to increase the power factor by eliminating capacitive and inductive impedance.

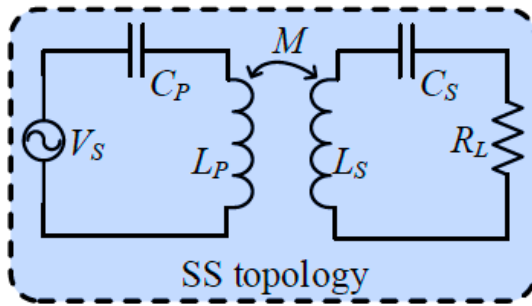


Figure 4.9: Series-Series Compensation topology.

The capacitance, internal resistance and inductance make up the circuit impedance. For the coils to resonate at the same frequency $X_C = X_L$, to ensure the the impedance of the circuit is only the resistance of the circuit.

$$\begin{aligned} X_C &= X_L \\ 2\pi f L &= \frac{1}{2\pi f C} \\ C &= \frac{1}{(2\pi f)(2\pi f)L} \end{aligned}$$

using the above equation, capacitance for the receiver and transmitter were calculated for three frequencies in the range 90kHz - 100kHz.

Table 4.3: Calculated capacitance for resonance.

Frequency	Capacitance [nF]
90kHz	158.6
95kHz	142.33
100kHz	128.5

For the capacitance values in Table 4.3. The impedance of the circuit will be purely resistive for the their respective frequencies. since $X_C = X_L$. The total impedance of the circuit is $Z = R + X_L - X_C = R$. Therefore maximum power factor will be achieved.

4.3.3 Rectifier

The rectifier converts the high frequency AC from the transmitter to DC for charging. The full-bridge rectifier will be used due to it's high efficiency and simple design. The diode used in the rectifier has to have a 3A maximum current capacity. Therefore 1N5401 Diodes will be used, with a 3A, 70V capacity.

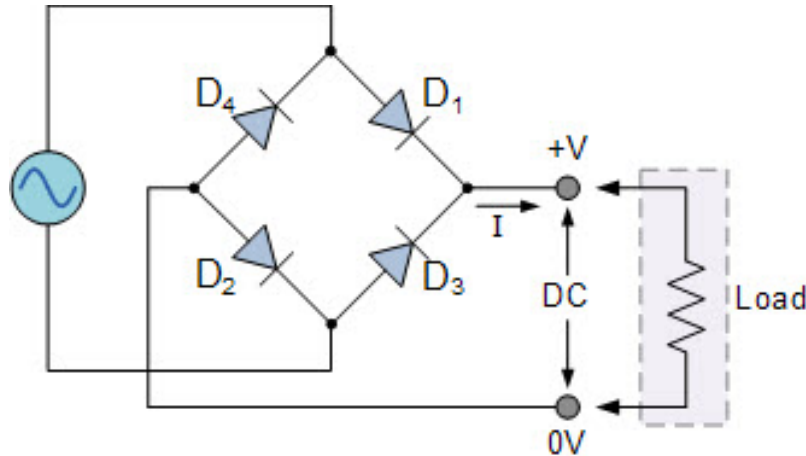


Figure 4.10: Full Bridge Rectifier.

The rectifier has a maximum efficiency of 81.2%. Needs four diode and a ripple factor of 0.48. To ensure that the ripple is filters out a large capacitor needs to be connected at output. The selected capacitance is $100\mu F$.

The full bridge rectifier was simulated in LT SPICE. The simulated circuit is illustrated in Figure 4.11. The switching frequency is set to 100kHz with an input voltage of 20V. To filter the output a large capacitor of $100\mu F$ was connected at the output. The output load was set to 10ohms.

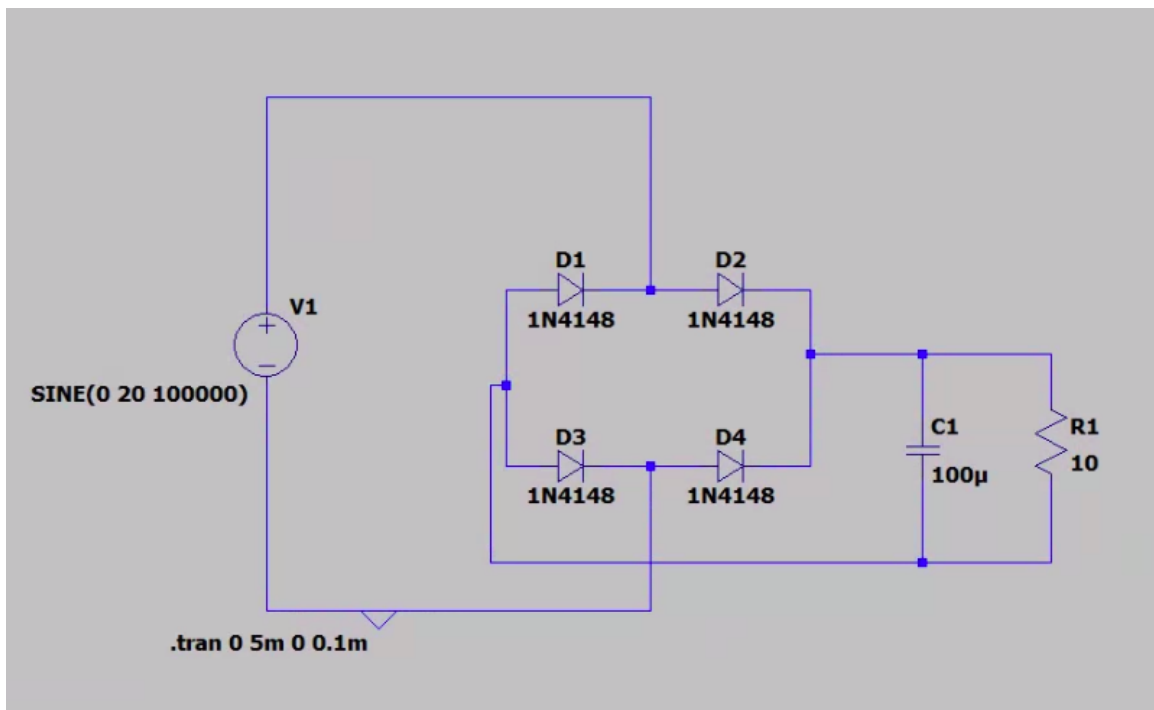


Figure 4.11: Full Bridge Rectifier in LT SPICE.

The output waveform is illustrated in Figure 4.12. The DC output was observed to be 13V.

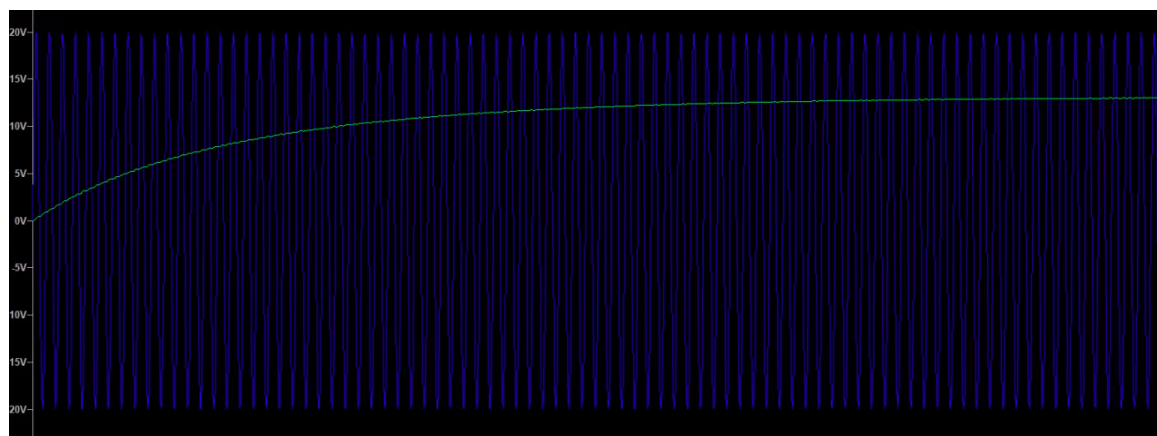


Figure 4.12: Full Bridge Rectifier Input and Output

4.3.4 Regulator

The linear voltage regulator will be used, due to it's low output ripple, fast response and availability in the Machines lab. The Voltage needs to be regulated at 15V. 15V is sufficient to charge the 12V battery without causing damage to the battery as can be seen from the battery's datasheet in Appendix D.

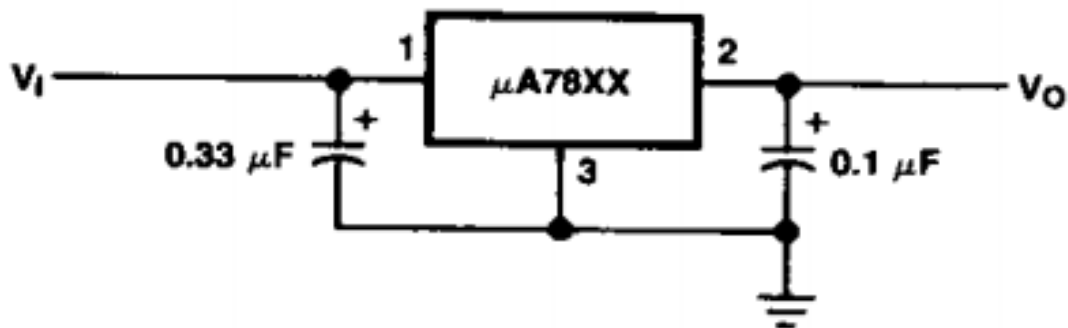


Figure 4.13: Voltage Regulator Circuit.

The linear regulator chosen is the UA7815UC. UA7815UC is rated at 1A and 15V. The circuit configuration for this voltage regulator can be seen in Figure 4.13. The regulator needs to be connected to a $330nF$ capacitor on the input and a $100nF$ at the output. As discussed in the literature review, the linear voltage regulator heats up and requires a heat sink. A heat sink will be used form the Machines lab.

Chapter 5

Results

5.1 Simulations

Two Software packages are used to simulate the wireless power transfer system. Firstly ANSYS Maxwell to determine the electromagnetic values of the system, Then LT Spice to predict power transmission.

5.1.1 ANSYS Maxwell

ANSYS Maxwell is a electromagnetic field simulation software for the design and analysis of electric motors, actuators, sensors, transformers and other electromagnetic and electro-mechanical devices. ANSYS Maxwell will be used to design the coils to determine the self inductance of the coils, mutual inductance between the coils, and coupling coefficient.

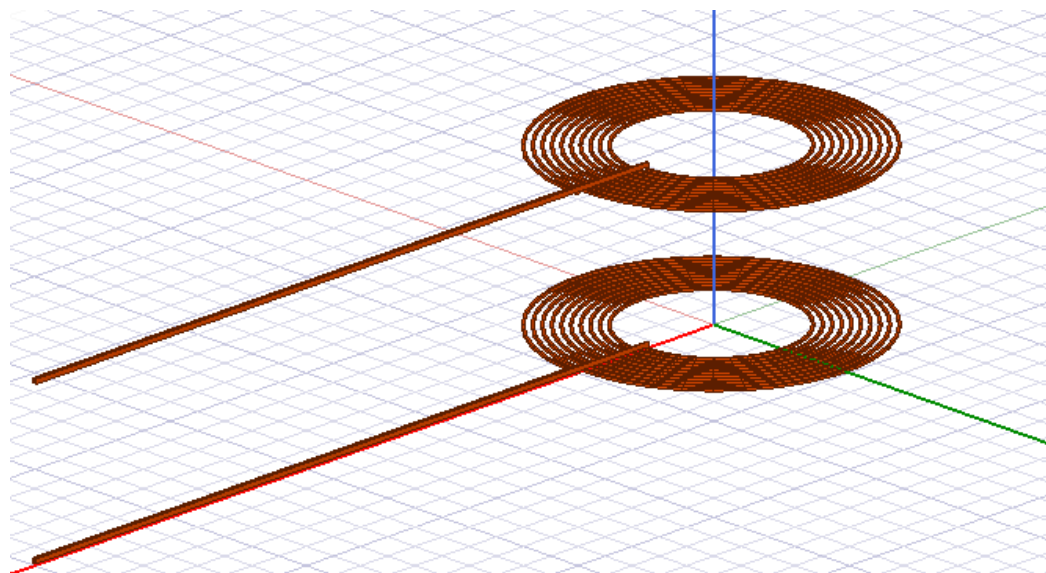


Figure 5.1: Coils designed in ANSYS

The transmitter and receiver coils have the same design. Figure 5.1 shows coils designed in ANSYS Maxwell. The coil has ten number of turns, 1.41mm wire diameter, 5mm radius change, 200mm coil outer diameter, and 100mm inner coil diameter. The distance between to coils will be varied from 10mm to 200mm.

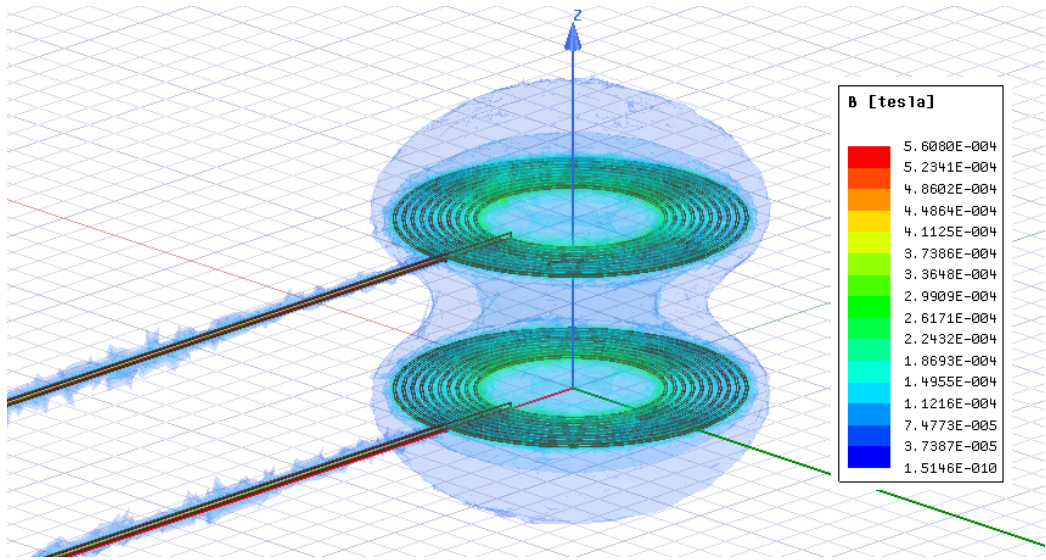


Figure 5.2: Magnetic field around the coils: B Field

The simulation was setup in 'magnetostatic' mode. The coils are excited with DC current to obtain the electro-magnetic parameters of the coils. A cubic meter box was made to simulate air around the coils. Figure 5.2, shows the resulting field from the coils. The field is represented as magnetic field strength in Tesla, the corresponding color coded values are shown in Figure 5.2.

From the simulation self inductance for both coils can be seen in Table 5.1. The Mutual inductance between the coils at 50mm transmission distance can also be seen in Table 5.1.

Table 5.1: Simulated Coil Parameters at 50mm transmission distance.

-	Transmitter	Receiver	Mutual
Inductance [uH]	19.54	19.55	5.68

The resulting coupling coefficient between the coils at 50mm transmission distance was determined to be 0.2912.

The simulation was ran for multiple transmission distances, Figure 5.3 shows how distance affects the Mutual inductance between the coils.

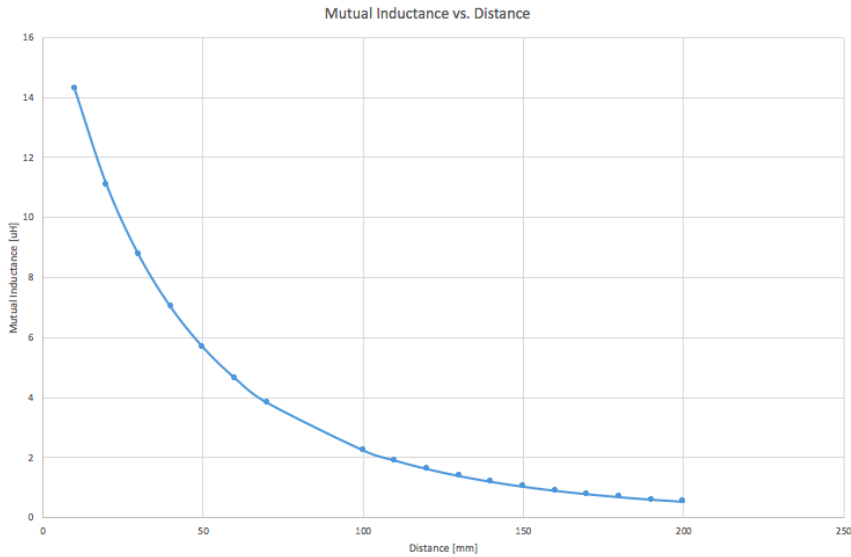


Figure 5.3: Mutual Inductance vs. Transmission Distance

Figure 5.4, show the relationship between transmission distance and the coupling coefficient. transmission distance was varied from 10mm to 200mm for both Mutual inductance and Coupling coefficient.

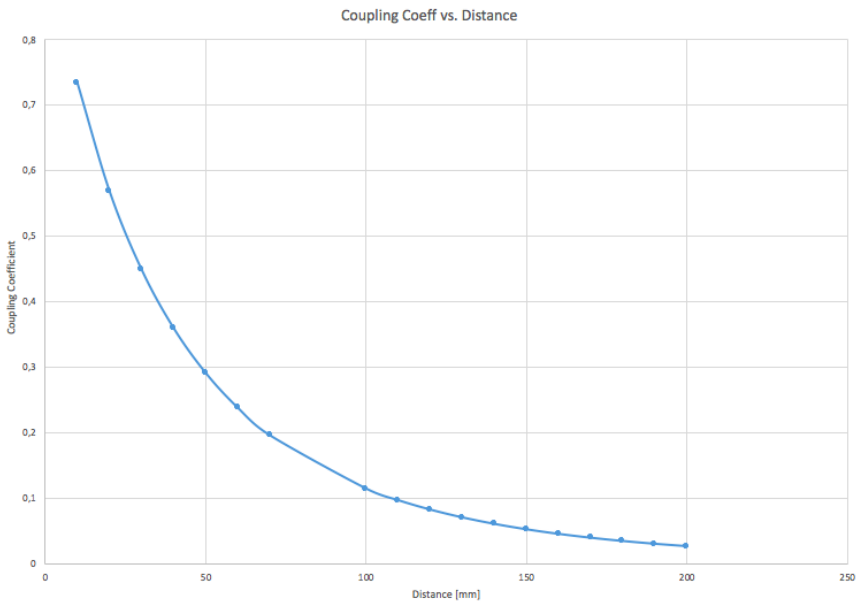


Figure 5.4: Coupling Coefficient vs. Transmission Distance.

5.1.2 LT Spice

LT Spice is a high performance SPICE simulation software, schematic capture and waveform viewer with enhancements and models for easing the simulation of analog circuits.

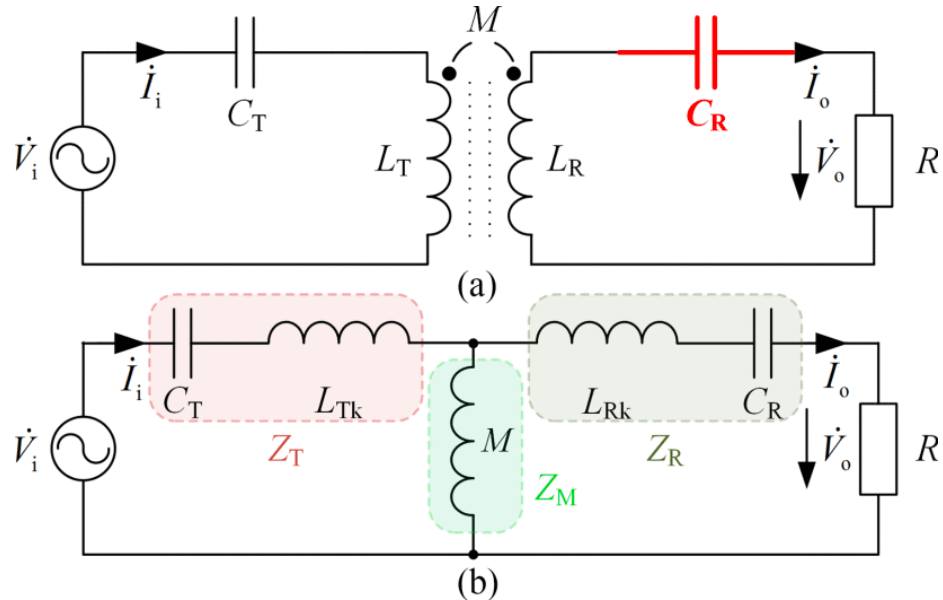


Figure 5.5: SS Compensated WPT system and it's equivalent T-Model.

To simulate the coils to obtain the power transfer characteristics the T-Model in Figure 5.5 is used. Where C_T and C_R are the transmitter capacitance and receiver capacitance respectively, M is the Mutual inductance, L_R and L_T are the receiver and transmitter inductance, $L_{TK} = L_T - M$ and $L_{RK} = L_R - M$ and R is the load resistance.

Parameter from simulations and calculation can be seen in Table 5.2. These are used to simulate power transmission of the system in LT Spice as can be seen in Figure 5.6

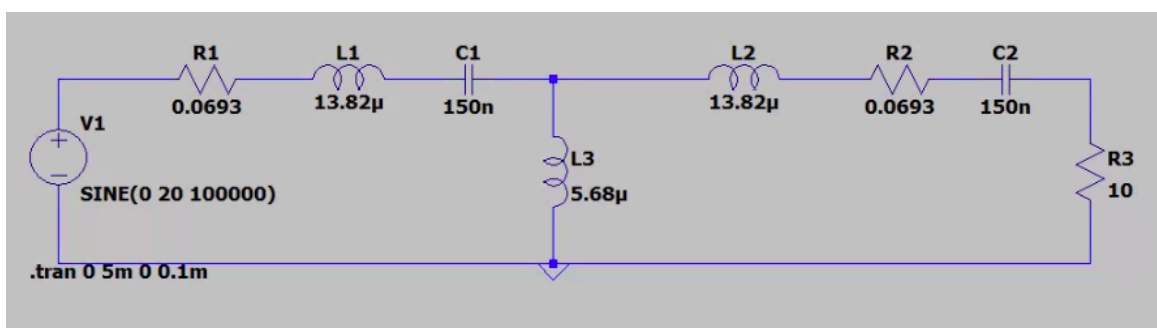


Figure 5.6: Equivalent T-model for the Coils

Table 5.2: Parameter for LT Spice simulation for 50mm transmission distance.

Parameters	
V_S	20 V
f	100 kHz
R_L	10 ohms
M	5.68 uH
$L_T = L_R$	19.5 uH
$L_{TK} = L_{RK}$	13.82 uH
$C_T = C_R$	150nF

The circuit in Figure 5.6 was simulated and the resulting output voltage was 33V from a supply of 20V. The waveforms can be seen in Figure 5.7. Where the green waveform is the 20V supply and the blue waveform is the 33V output.

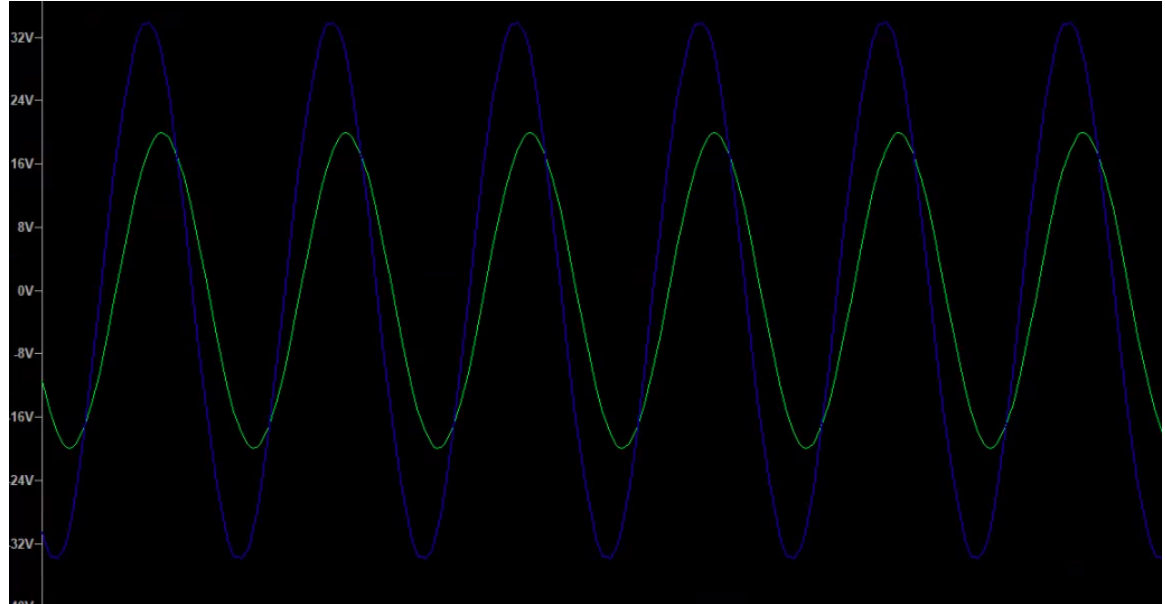


Figure 5.7: Input (green) and Output (blue) Voltage for 50mm

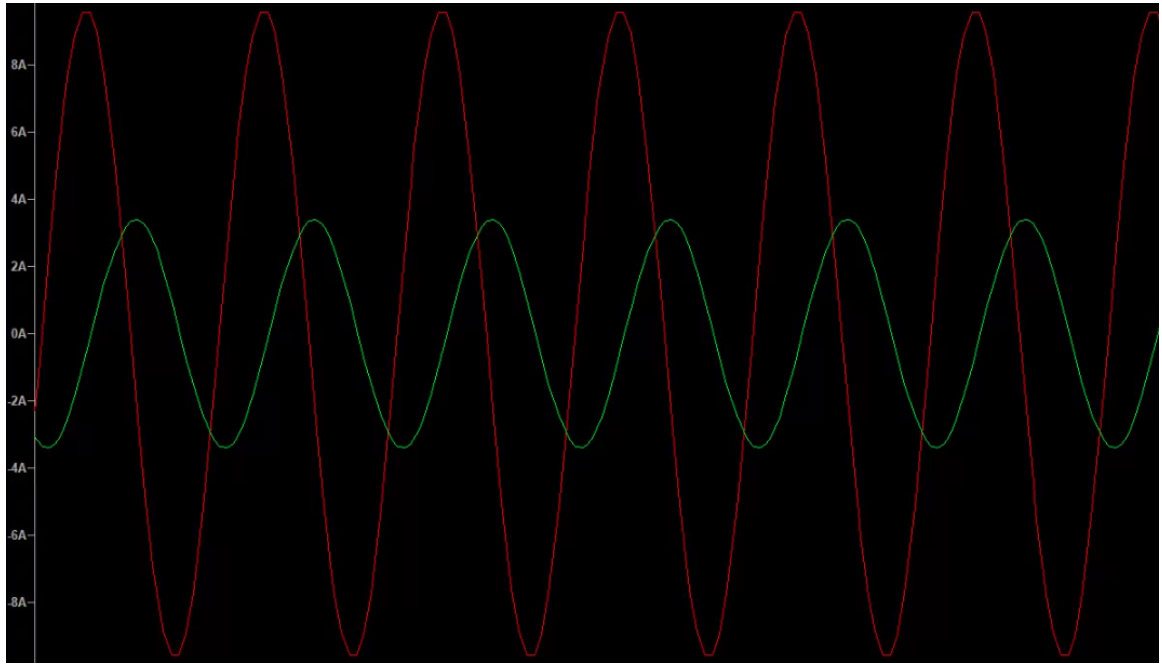


Figure 5.8: Input (red) and Output (green) Current for 50mm

The input and output current for 10 ohms load can be seen in Figure 5.8. The input current is 9.5A and the output current is 3.3A. Their waveforms can be seen in Figure 5.8, where Input current is red and output is green.

Table 5.3: Power transmission for 50mm

-	Voltage [V]	Current [A]	Power [W]
Input	20	9.5	190
Output	33	3.3	108.9

From the power calculated in Table 5.3, efficiency of the system for a 10 ohm load was calculated to be 57.3%.

The Simulation was repeated for Transmission distance of 100mm with a mutual inductance of 2.244uH. The circuit in Figure 5.6 was simulated with the values for a transmission distance of 100mm and the resulting output voltage was 15.5V from a supply of 20V. The waveforms can be seen in Figure 5.9. Where the blue waveform is the 20V supply and the green waveform is the 9V output.

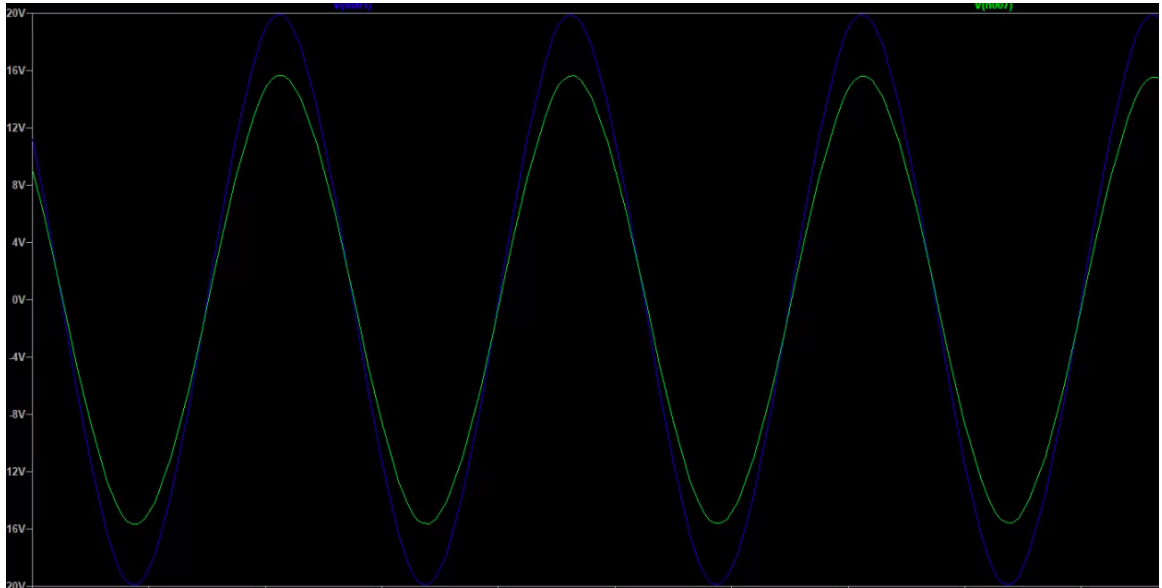


Figure 5.9: Input (blue) and Output (green) Voltage for 100mm



Figure 5.10: Input (red) and Output (green) Current for 100mm

The input and output current for 10 ohms load can be seen in Figure 5.10. The input current is 11A and the output current is 1.5A. Their waveforms can be seen in Figure 5.10, where Input current is blue and output is green.

From the power calculated in Table 5.4, efficiency of the system for a transmission distance of 100mm was calculated to be 10.57%.

Table 5.4: Power transmission for a 10 ohm load

-	Voltage [V]	Current [A]	Power [W]
Input	20	11	220
Output	15.5	1.5	23.25

5.2 Practical Experimentation

The LCR meter in the Machines lab was used to measure the actual inductance and internal resistance of the coils. Table 5.5, shows the measured values.

Table 5.5: Measured Coil Parameters

	Transmitter	Receiver
Self Inductance [uH]	19.72	18.42
Internal Res [Ohms]	0.0697	0.0583

From the actual coil inductance values, the capacitance values needed for resonance can be calculated. As mentioned in the design, for resonance to occur the capacitive elements must eliminate the inductive elements of the circuit. That means $X_C = X_L$.

The capacitance was calculated for a switching frequency of 90kHz. C_1 and C_2 were calculated to be 158.6nF and 137.5nF, the closest capacitance value found in the lab for both was 150nF. The new switching frequency was calculated to between 93kHz and 97kHz

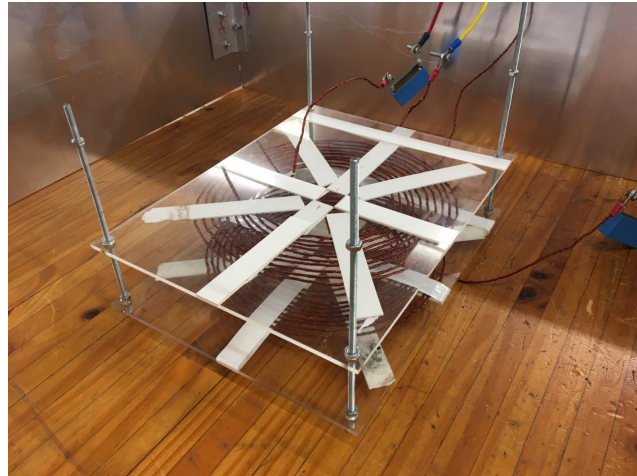


Figure 5.11: Coils

Different experiments are performed to observe the effects of certain parameters on the system's transmission efficiency. The parameters that were considered are load impedance, transmission distance, switching frequency and input voltage.

5.2.1 Experiment 1: Transmission distance

For this experiment input voltage was kept constant at 10V and a constant switching frequency of 100kHz was supplied. The distance was varied from 50mm to 120mm, the results are shown in Table 5.6.

Table 5.6: Input and Output for different transmission distances with 10V input voltage and 100kHz switching frequency.

Distance	Input Current	Output Voltage	Output Current
50 mm	3.44 A	14.4 V	1.3 A
100 mm	2.80 A	6.8 V	0.5 A
120 mm	2.30 A	4.60 V	0.1 A

The efficiency as distance changes is plotted in Figure 5.12. It can be observed that the efficiency increases as distance is decreases. This is expected because the magnetic field weakens as the distance from the transmitter coil increases, hence the induced power in the receiver coil decreases.

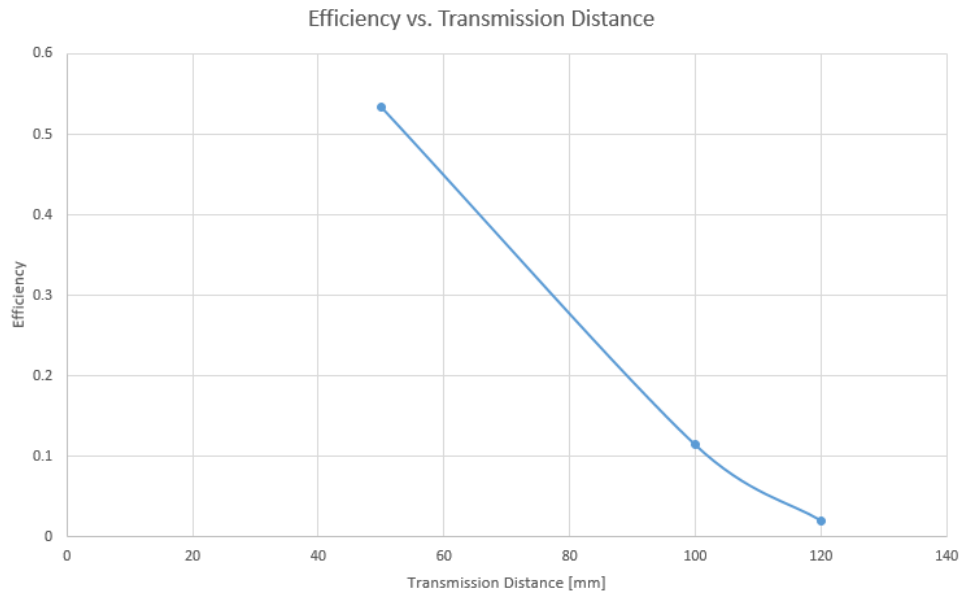


Figure 5.12: Transmission Efficiency vs. Transmission Distance

5.2.2 Experiment 2: Switching Frequency

For this experiment input voltage was kept constant at 10V and The Experiment to two transmission distances: 50mm and 100mm. The switching frequency was varied from 93kHz to 100kHz, The results for a transmission distance for 50mm are shown in Table 5.7.

Table 5.7: Input and Output for different switching frequencies at 50mm.

Frequency	Input Current	Output Voltage	Output Current
100kHz	0.75 A	2.2 V	0.1 A
97kHz	1 A	2.7 V	0.1 A
95kHz	1.12 A	3 V	0.2 A
93kHz	1.13 A	2.9 V	0.2 A

The efficiency increases when it moves closer to 93kHz. Therefore it is clear the 95kHz is the resonance frequency, as can be seen in Figure 5.13. This is expected, because 95kHz is the resonant frequency - meaning that it has the optimal power factor and therefore the maximum efficiency.

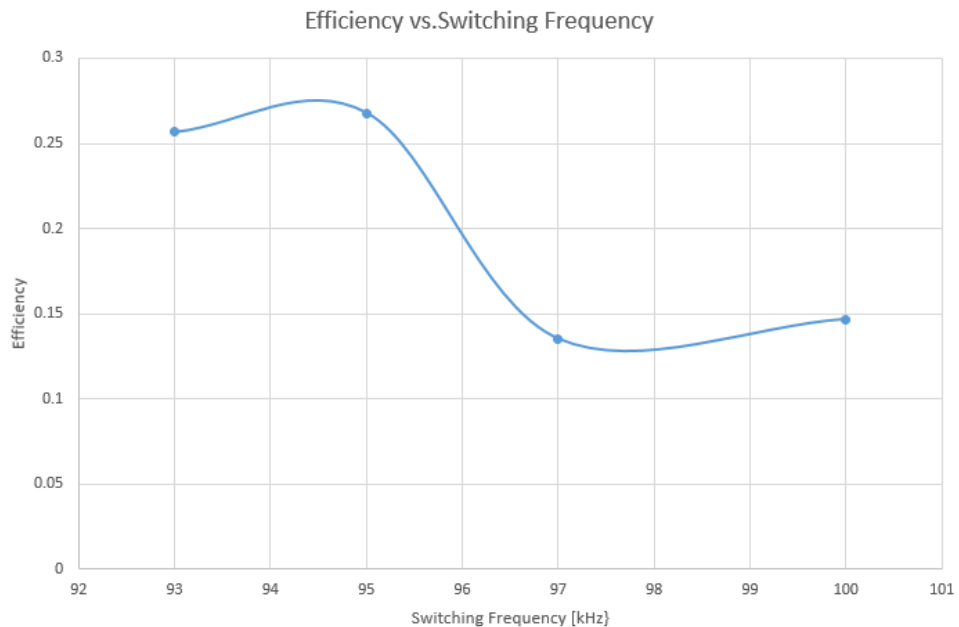


Figure 5.13: Transmission Efficiency vs. Switching Frequency for 50mm

When the experiment was repeated for a different transmission distance of 100mm, The resulting plot followed similar trend as the when the distance was 50mm, as can be seen in Figure 5.14.

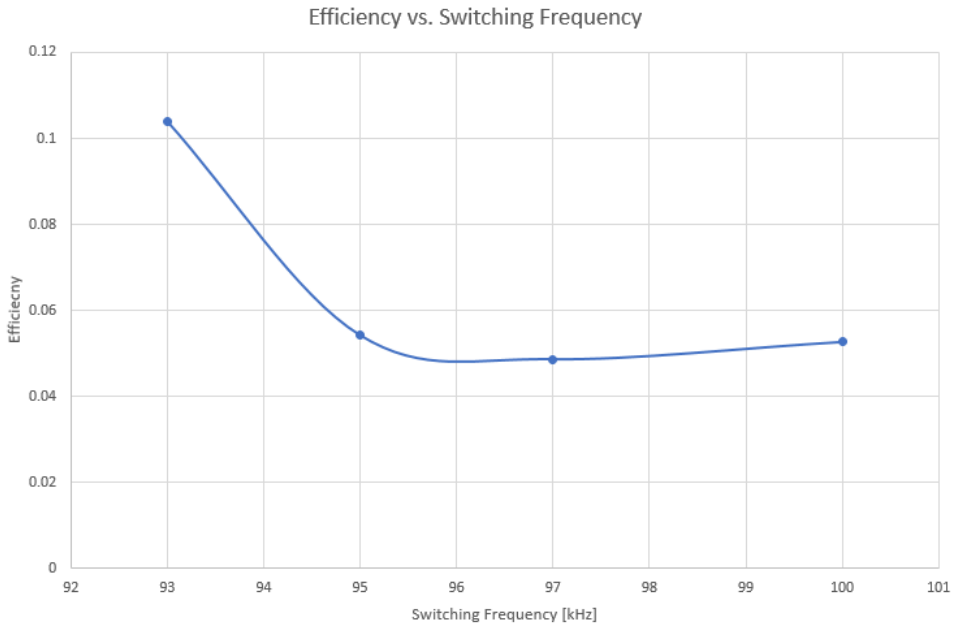


Figure 5.14: Transmission Efficiency vs. Switching Frequency for 100mm

5.2.3 Experiment 3: Load

For this experiment input voltage was kept constant at 5V and the experiment was conducted for two transmission distance which are 50mm and 100mm. Switching frequency was also kept constant at 100kHz. The Load Resistance was varied from 5ohms to 20ohms, The results for the transmission distance of 50mm are shown in Table 5.8.

Table 5.8: Input and Output for different Load impedance for 50mm.

Load	Input Current	Output Voltage	Output Current
5 ohms	1.47 A	4.3 V	0.7 A
10 ohms	1.77 A	6.6 V	0.6 A
15 ohms	1.88 A	7.8 V	0.4 A
20 ohms	1.92 A	8.6 V	0.3 A

The efficiency as distance changes is plotted in Figure 5.15. It can be observed that the efficiency decreases as the load is increases.



Figure 5.15: Transmission Efficiency vs. Load Resistance for 50mm

When the experiment was repeated for a different transmission distance of 100mm, The resulting plot followed similar trend as the when the distance was 50mm, as can be seen in Figure 5.16.

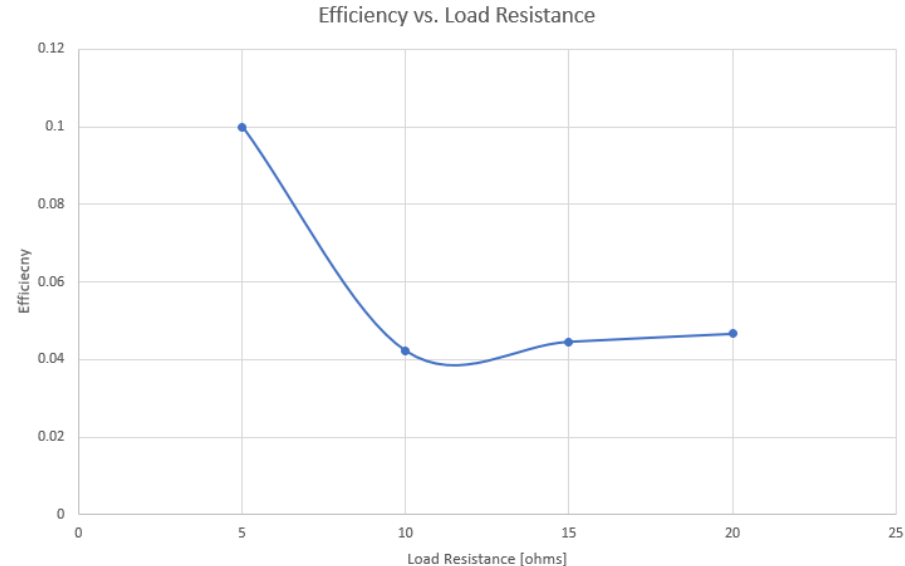


Figure 5.16: Transmission Efficiency vs. Load Resistance for 100mm

5.2.4 Experiment 4: Input Voltage

Input voltage was varied from 2V to 12V, while transmission distance, Switching Frequency, and load resistance were kept constant at 50mm, 100kHz and 10ohm respectively. The resulting trend can be seen in Figure 5.17. The experiment was repeated for a transmission distance of 100mm.

Table 5.9: Input and Output for 50mm at 100kHz

Input Voltage	Input Current	Output Voltage	Output Current
2 V	0.75 A	2.1 V	0.2 A
5 V	1.77 A	6.6 V	0.6 A
8 V	2.77 A	11.1 V	1 A
10 V	3.44 A	14.14 V	1.3 A
12 V	4.05 A	16.9 V	1.6 A

The efficiency as input voltage changes is plotted in Figure 5.17. The observed trend showed that efficiency increased as input voltage increase.

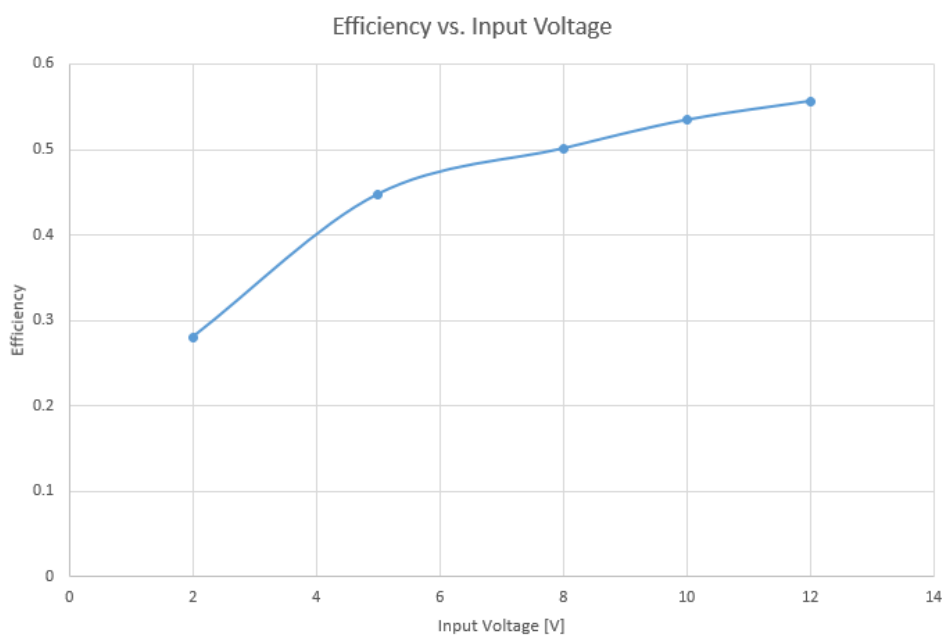


Figure 5.17: Transmission Efficiency vs. Input Voltage, for 50mm

When the experiment was repeated for a different transmission distance of 100mm, The resulting plot followed similar trend as the when the distance was 50mm, as can be seen in Figure 5.18.

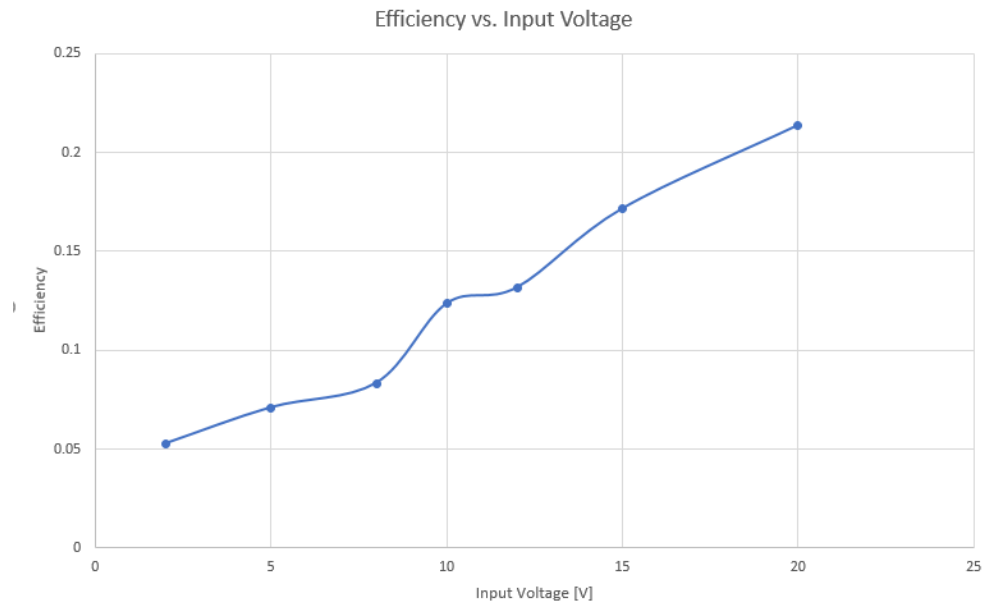


Figure 5.18: Transmission Efficiency vs. Input Voltage, for 100mm

5.2.5 Mutual inductance calculations

The mutual inductance between the coils is calculated used the following equation [34].

$$M_{12} = \frac{V_2}{V_1} L_1 \quad (5.1)$$

where V_2 as the receiver voltage, V_1 is the transmitter voltage, and L_1 is the inductance of the transmitter coil. Mutual inductance is calculated for the results of experiment 1. The resulting mutual inductance can been seen in Table 5.10

Table 5.10: Practical Mutual Inductance for different distances

Distance	Mutual Inductance [uH]
50 mm	28.4
100 mm	13.4
120 mm	9

5.2.6 Charging 12V Battery

For the 12V battery to be charged a charging method would have to be designed as the output from the WPT system can not be connected directly to the battery. The bike battery is a 12V38AH/20HR lead-acid battery as can be seen in Figure 5.19.



Figure 5.19: Electric bike Battery

The charging methods discussed in the literature review could not be implemented due to time constraints.

Chapter 6

Discussion

This section deals with discussion of results obtained. How they are inline with theory and explanation of any variations.

6.1 Self Inductance

The self inductance of the coils was calculated using knowledge from the literature reviewed, simulated using ANSYS Maxwell software and measured using an LCR meter from the machines lab. Table 6.1, compare all three methods used to obtain the inductance of the coils.

Table 6.1: Self Inductance from different methods.

-	Transmitter [uH]	Receiver [uH]
Calculated	19.01	19.01
Simulated	19.5	19.5
Measured	19.72	18.42

The many factor that could have contributed to the different inductance value from the different methods. Firstly, the spacing between turns on the actual coil is inconsistent. Secondly, the rest of the wire coil dimensions are not exact, this is because the wire had to be made into a circle manually and there was error in the implementation. Thirdly, the actual coil was in a Litz configuration, the calculation and simulation offered no way to account for this configuration.

6.2 Mutual Inductance

The mutual inductance between the coils was simulated for multiple distance using ANSYS Maxwell and Calculate from experimental results for different transmission distances using knowledge from the literature surveyed. Table 6.2, compares both methods used to obtain the mutual inductance between the coils.

Table 6.2: Mutual Inductance from different methods.

	50mm	100mm	120mm
Calculated	28.4uH	13.4uH	9uH
Simulated	5.68uH	2.24uH	1.62uH

Mutual Inductance is the interaction of one coils magnetic field on another coil as it induces a voltage in the other coil. When the coils are close then most of the magnetic flux generated will interact with the other coil. When the distance between the coils increases, the interaction between the two decreases. Therefore Mutual inductance should decrease as distance between the coils increases. The simulated and calculated values for mutual inductance are inline with the relationship.

The simulated value are different for a number of reasons. Fast switching circuits face a common problem of switching noise. When switching a MOSFET its body diode and reactive elements result in overshooting of current and voltage. This is called ringing. Figure 6.1, shows the resulting waveform from the implemented inverter with ringing. Ringing will result in higher voltages being outputted by the rectifier than the input. This switching noise, produces incorrect mutual inducances on for the practical results. Methods to reduce ringing were not investigated due to time constraints.

The simulation - as stated in section 6.1, did not consider the Litz configuration. Simulations are generally in ideal situations as many factors can not be considered.

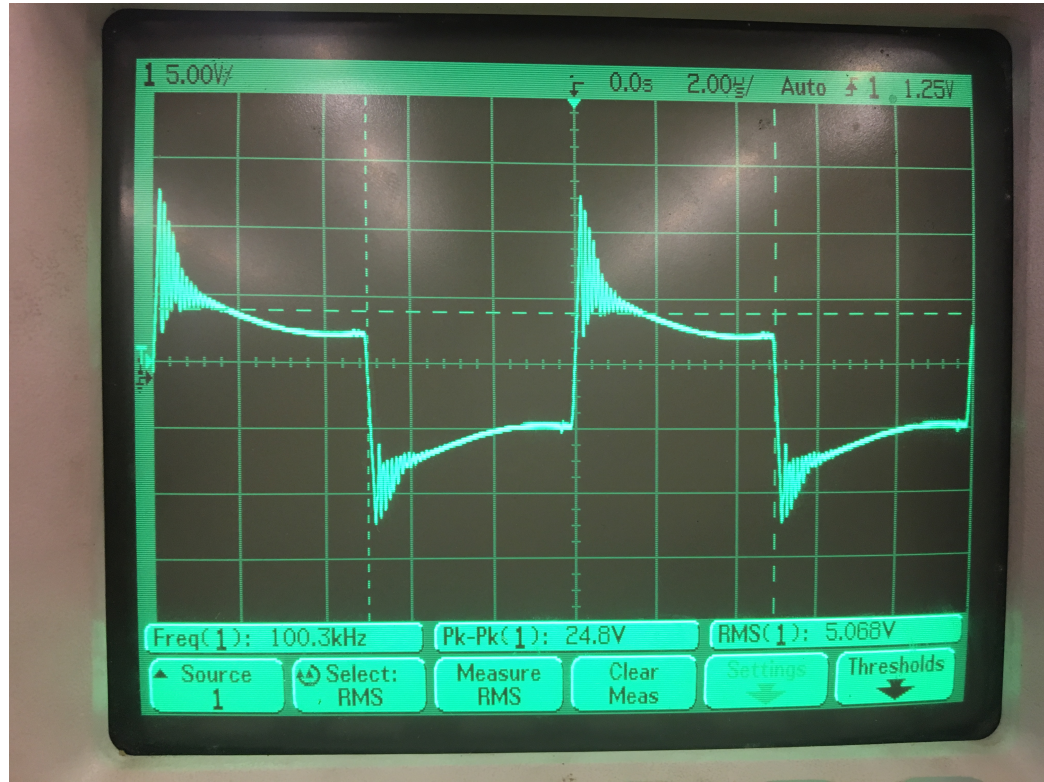


Figure 6.1: Ringing graph from inverter

6.3 Transmission Distance

In Table 6.3, efficiency is observed to drop from 54% to 12% when transmission distance went from 50mm to 100mm.

Results from Experiment 1 in section 5.2.1, show that efficiency decreases exponentially with an increase in transmission distance. This is inline with the theory from the review literature. From theory, this happens as a result of a exponential decrease in mutual inductance as seen in the previous section, mutual inductance is inversely proportional to transmission distance and directly proportional to efficiency. Therefore an increase in distance results in an exponential decrease in efficiency.

The efficiency values for transmission distance of 50mm and 100mm are close to the efficiencies simulated in LT spice. LT spice efficiency for 50mm and 100mm was 57% and 10.57% respectively.

Table 6.3: Efficiency for different transmission distances with 10V input voltage and 100kHz switching frequency.

Distance	Efficiency
50 mm	54%
100 mm	12%
120 mm	2%

6.4 Switching Frequency

Results from Experiment 2 showed that the efficiency at 100mm transmission distance was the highest. The results have been summarised in Table 6.4.

Table 6.4: Efficiency for different switching frequencies

Frequency	Efficiency
100kHz	5.3%
97kHz	4.9%
95kHz	5.5%
93kHz	10.5%

Theory suggested that at resonance the system would have the optimal efficiency, because the circuit would be purely resistive with no reactive elements. This would result in optimal power factor and therefore optimal efficiency. The results from experiment 2 are inline with the theory predictions.

Chapter 7

Conclusion

The main objective of this study was to design implement a wireless power transfer system to charge a 12V battery for an electric bike. This was achieved by reviewing literature of state of the art wireless power transfer systems for electric bikes. From the literature theory was developed to design and implement the WPT system.

Experiments were performed to evaluate the implemented system. Four experiment were performed to observe the effect of certain parameter of the system transmission efficiency. These parameter are - transmission distance, load resistance, switching frequency and input voltage.

The coils were successfully built, where the transmitter coil had an inductance of 19.72uH and the receiver coil had an inductance of 18.42uH. From simulations, the mutual inductance between the coils for a transmission distance of 50mm was 5.68uH and for a transmission distance of 100mm it was 2.244uH. The practical mutual inductances were inaccurate due to switching noise from the mosfets in the inverter circuit.

The transmission efficiency for transmission distance of 50mm was 54% and for a transmission distance of 100mm it was 12%. Therefore to charge the 12V battery at 100mm the input voltage had to be 20V, 4A to output 14.5V, 1A for a 10ohm load.

The system could not be connected directly to the battery for charging because the charging technique (CV/CC, CC, or CV) could not be implemented in time.

Chapter 8

Recommendations

8.1 Resonance

Perform experiments with more frequencies around the calculated resonance frequency to find the exact resonant frequency for the practical system. This will improve the efficiency of the system.

8.2 Switching noise

Implement circuitry to reduce switching noise to make the system more accurate and predictable.

8.3 Charging Method

Implement a charging mechanism to allow the WPT system to be tested on an actual battery. This will allow for the system to be properly evaluated for the application it was intended for, which is to wirelessly transfer power to charge an electric bike.

8.4 Communication Protocol

Currently, if a receiver coil is close to the transmitter coil and the power is on, power will be transferred. For security purposes each coil can have an identification tag (RFID), to allow more control over who can charge.

An example could be in a parking lot at a mall where they install WPT chargers. The communication can be used for checking if someone has payed for charging.

8.5 Alignment

For optimal power transfer, the transmitter and receiver coils should be properly aligned. When placing your electric bike for charging - perfect alignment might be an impossible task.

To assist, an application could be developed to guide the user while parking to place the bike such that the coils are perfectly aligned.

Bibliography

- [1] Z. Zhang, H. Pang, A. Georgiadis, and C. Cecati, “Wireless power transfer - an overview,” *IEEE Transactions on Industrial Electronics*, pp. 1–1, 2018.
- [2] X. Mou and H. Sun, “Wireless power transfer: Survey and roadmap,” in *2015 IEEE 81st Vehicular Technology Conference (VTC Spring)*, May 2015, pp. 1–5.
- [3] F. Pellitteri, V. Boscaino, A. O. D. Tommaso, R. Miceli, and G. Capponi, “Inductive power transfer for 100w battery charging,” in *IECON 2013 - 39th Annual Conference of the IEEE Industrial Electronics Society*, Nov 2013, pp. 894–899.
- [4] V. Castiglia, L. D. Noia, P. Livreri, R. Miceli, C. Nevoloso, F. Pellitteri, and F. Viola, “An efficient wireless power transfer prototype for electrical vehicles,” in *2017 IEEE 6th International Conference on Renewable Energy Research and Applications (ICRERA)*, Nov 2017, pp. 1215–1220.
- [5] L. Xie, Y. Shi, Y. T. Hou, and A. Lou, “Wireless power transfer and applications to sensor networks,” *IEEE Wireless Communications*, vol. 20, no. 4, pp. 140–145, August 2013.
- [6] O. Jonah and S. V. Georgakopoulos, “Wireless power transfer in concrete via strongly coupled magnetic resonance,” *IEEE Transactions on Antennas and Propagation*, vol. 61, no. 3, pp. 1378–1384, March 2013.
- [7] E. Elkhouly and S. Yang, “Transmitter coil design for resonant wireless power transfer,” in *2016 IEEE PELS Workshop on Emerging Technologies: Wireless Power Transfer (WoW)*, Oct 2016, pp. 1–5.
- [8] X. Shi, C. Qi, M. Qu, S. Ye, G. Wang, L. Sun, and Z. Yu, “Effects of coil shapes on wireless power transfer via magnetic resonance coupling,” vol. 28, 05 2014.
- [9] Y. Cheng and Y. Shu, “A new analytical calculation of the mutual inductance of the coaxial spiral rectangular coils,” *IEEE Transactions on Magnetics*, vol. 50, no. 4, pp. 1–6, April 2014.

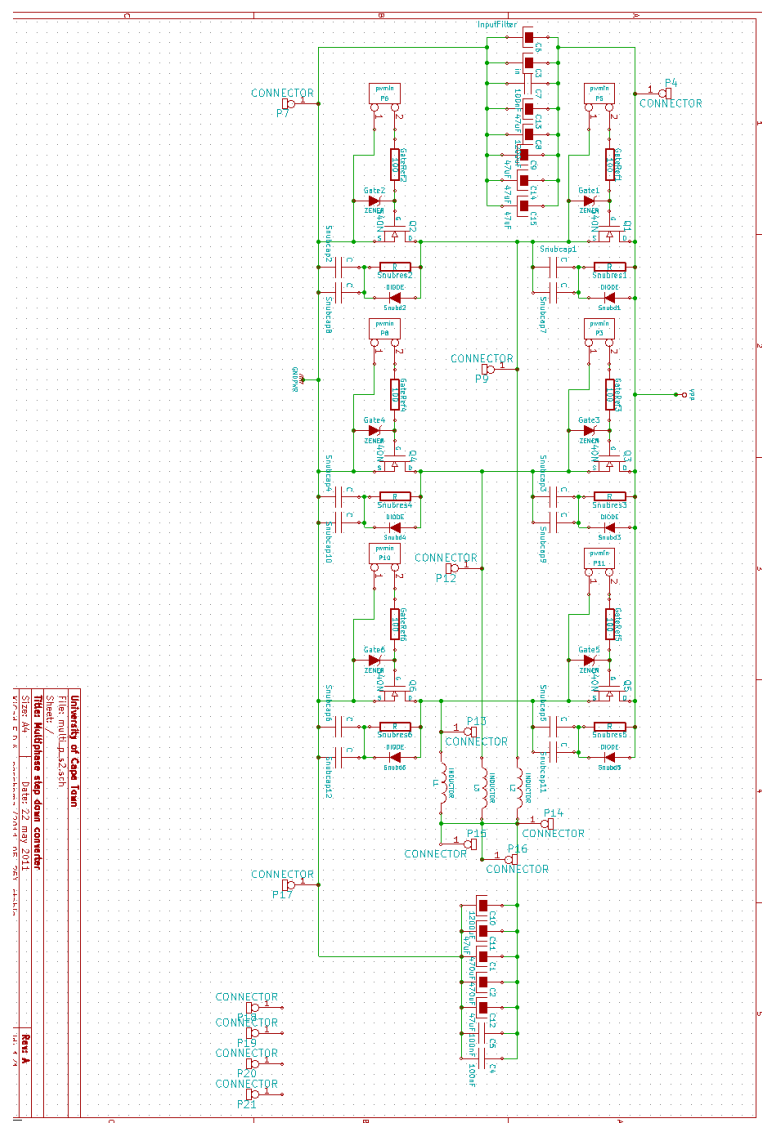
- [10] A. Kurs, A. Karalis, R. Moffatt, J. D. Joannopoulos, P. Fisher, and M. Soljačić, "Wireless power transfer via strongly coupled magnetic resonances," *Science*, vol. 317, no. 5834, pp. 83–86, 2007. [Online]. Available: <http://science.sciencemag.org/content/317/5834/83>
- [11] D. W. Kim, Y. D. Chung, H. K. Kang, C. Y. Lee, H. M. Kim, H. C. Jo, Y. J. Hwang, J. Y. Jang, and Y. S. Yoon, "Effects and properties of contactless power transfer for hts receivers with four-separate resonance coils," *IEEE Transactions on Applied Superconductivity*, vol. 23, no. 3, pp. 5 500 404–5 500 404, June 2013.
- [12] S. Y. Hui, "Planar wireless charging technology for portable electronic products and qi," *Proceedings of the IEEE*, vol. 101, no. 6, pp. 1290–1301, June 2013.
- [13] A. Christ, M. Douglas, J. Nadakuduti, and N. Kuster, "Assessing human exposure to electromagnetic fields from wireless power transmission systems," *Proceedings of the IEEE*, vol. 101, no. 6, pp. 1482–1493, June 2013.
- [14] A. P. Sample, B. H. Waters, S. T. Wisdom, and J. R. Smith, "Enabling seamless wireless power delivery in dynamic environments," *Proceedings of the IEEE*, vol. 101, no. 6, pp. 1343–1358, June 2013.
- [15] Q. Yuan, Q. Chen, L. Li, and K. Sawaya, "Numerical analysis on transmission efficiency of evanescent resonant coupling wireless power transfer system," *IEEE Transactions on Antennas and Propagation*, vol. 58, no. 5, pp. 1751–1758, May 2010.
- [16] J. Kim, J. Kim, S. Kong, H. Kim, I. Suh, N. P. Suh, D. Cho, J. Kim, and S. Ahn, "Coil design and shielding methods for a magnetic resonant wireless power transfer system," *Proceedings of the IEEE*, vol. 101, no. 6, pp. 1332–1342, June 2013.
- [17] W. X. Zhong, X. Liu, and S. Y. R. Hui, "A novel single-layer winding array and receiver coil structure for contactless battery charging systems with free-positioning and localized charging features," *IEEE Transactions on Industrial Electronics*, vol. 58, no. 9, pp. 4136–4144, Sept 2011.
- [18] S. Y. R. Hui and W. C. Ho, "A new generation of universal contactless battery charging platform for portable consumer electronic equipment," in *2004 IEEE 35th Annual Power Electronics Specialists Conference (IEEE Cat. No.04CH37551)*, vol. 1, June 2004, pp. 638–644 Vol.1.

- [19] U. Reggiani, G. Grandi, G. Sancinetto, and G. Serra, "Comparison between air-core and laminated iron-core inductors in filtering applications for switching converters," in *7th IEEE International Power Electronics Congress. Technical Proceedings. CIEP 2000 (Cat. No.00TH8529)*, Oct 2000, pp. 9–14.
- [20] Y. Li, X. Li, F. Peng, H. Zhang, W. Guo, W. Zhu, and T. Yang, "Wireless energy transfer system based on high q flexible planar-litz mems coils," in *The 8th Annual IEEE International Conference on Nano/Micro Engineered and Molecular Systems*, April 2013, pp. 837–840.
- [21] T. Mizuno, S. Yachi, A. Kamiya, and D. Yamamoto, "Improvement in efficiency of wireless power transfer of magnetic resonant coupling using magnetoplated wire," *IEEE Transactions on Magnetics*, vol. 47, no. 10, pp. 4445–4448, Oct 2011.
- [22] Z. Pantic and S. Lukic, "Computationally-efficient, generalized expressions for the proximity-effect in multi-layer, multi-turn tubular coils for wireless power transfer systems," *IEEE Transactions on Magnetics*, vol. 49, no. 11, pp. 5404–5416, Nov 2013.
- [23] B. J. Varghese, P. B. Bobba, and M. Kavitha, "Effects of coil misalignment in a four coil implantable wireless power transfer system," in *2016 IEEE 7th Power India International Conference (PIICON)*, Nov 2016, pp. 1–6.
- [24] S. R. Cove, M. Ordóñez, N. Shafiei, and J. Zhu, "Improving wireless power transfer efficiency using hollow windings with track-width-ratio," *IEEE Transactions on Power Electronics*, vol. 31, no. 9, pp. 6524–6533, Sept 2016.
- [25] S. Moon, B. Kim, S. Cho, and G. Moon, "Analysis and design of wireless power transfer system with an intermediate coil for high efficiency," in *2013 IEEE ECCE Asia Downunder*, June 2013, pp. 1034–1040.
- [26] Z. Ye, Y. Sun, X. Dai, C. Tang, Z. Wang, and Y. Su, "Energy efficiency analysis of u-coil wireless power transfer system," *IEEE Transactions on Power Electronics*, vol. 31, no. 7, pp. 4809–4817, July 2016.
- [27] C. Jiang, K. T. Chau, C. Liu, and C. H. T. Lee, "An overview of resonant circuits for wireless power transfer," *Energies*, vol. 10, no. 7, 2017. [Online]. Available: <http://www.mdpi.com/1996-1073/10/7/894>
- [28] R. Mai, Y. Chen, Y. Li, Y. Zhang, G. Cao, and Z. He, "Inductive power transfer for massive electric bicycles charging based on hybrid topology switching with a single

- inverter,” *IEEE Transactions on Power Electronics*, vol. 32, no. 8, pp. 5897–5906, Aug 2017.
- [29] W. Yan and J. Chen, “A general design of magnetic coupling resonant wireless power transmission circuit,” vol. 69, p. 012197, 06 2017.
- [30] A. Zainuddin, F. Radzi, M. Mat ibrahim, and N. Abdul Hamid, “A development of electrical vehicle charging system using wireless power transfer,” vol. 11, pp. 6328–6333, 05 2016.
- [31] C. Nataraj, “Resonant coils analysis for inductively coupled wireless power transfer applications,” 07 2016.
- [32] Z. Wang and X. Wei, “Design considerations for wireless charging systems with an analysis of batteries,” *Energies*, vol. 8, no. 10, pp. 10 664–10 683, 2015. [Online]. Available: <http://www.mdpi.com/1996-1073/8/10/10664>
- [33] S. Chhawchharia, S. K. Sahoo, M. Balamurugan, S. Sukchai, and F. Yanine, “Investigation of wireless power transfer applications with a focus on renewable energy,” *Renewable and Sustainable Energy Reviews*, vol. 91, pp. 888 – 902, 2018. [Online]. Available: <http://www.sciencedirect.com/science/article/pii/S1364032118303162>
- [34] E. R. Joy, A. Dalal, and P. Kumar, “Accurate computation of mutual inductance of two air core square coils with lateral and angular misalignments in a flat planar surface,” *IEEE Transactions on Magnetics*, vol. 50, no. 1, pp. 1–9, Jan 2014.

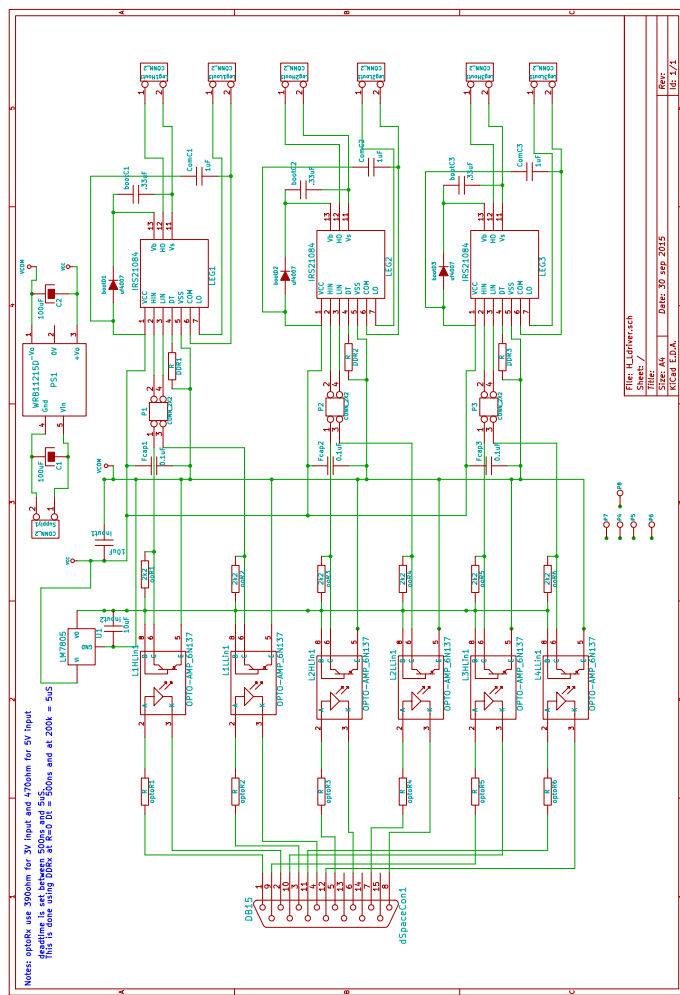
Appendix A

Inverter Circuit



Appendix B

Gate Driver Circuit



Appendix C

STM32: PWM Code

Click to see code in github.

Appendix D

12V Battery Datasheet

GS GREENSAVER CORPORATION **Silicone Power Battery**

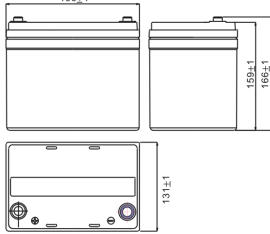
MODEL: SP38-12(38AH/20HR)



General Features

High Corrosion Resistart Performance:Pb-Ca multi-alloy grid
Patented Silicate Compound Electrolyte:Minor acid vapor, environment friendly.
High Energy Density and Power Density.
Excellent Charge Acceptance Ability.
Strong High and Low Temperature Performance.
Optimized Capability of Instant High-current Discharging

Outer Dimensions



Product Specification

Nominal Voltage:	12 V
Rated Capacity:	
20Hour Rate (1.9A to 10.5V)	38 AH
10Hour Rate (3.6A to 10.5V)	36 AH
5Hour Rate (6.45A to 10.5V)	32.25 AH
2Hour Rat (13.5A to 10.5V)	27 AH

Dimension and Weight

Length	196mm±1mm
Width	131mm±1mm
Height	159mm±1mm
Total Height	166mm±1mm
Weight(WT)	11.5kg

Internal Resistance: Fully charged Battery ≤15m Ω

Self discharge Rate:20°C, 4% first month, after 1% per month

Operating Temperature Range:

Discharge	-35°C(-31°F) ~50°C(122°F)
Charge	-15°C (5°F)~40°C(104°F)
Storage	-15°C(5°F)~40°C(104°F)

Charging Methods:

Floating Use	13.5V~13.8V(20°C), Compensation coefficient-3mv/cell/°C
Cycling Use	14.4V~15.0V(20°C), Compensation coefficient-5mv/cell/°C
Max Charge Current	0.3C(A)

Case

ABS

Applications

Electric Vehicle, Solar power, Wind power, Telecom Systems, UPS

